


Catchment response to climate change under CMIP6 scenarios: a case study of the Krishna River Basin

Suram Anil , Anand Raj P and Vamsi Krishna Vema

Department of Civil Engineering, National Institute of Technology Warangal, Warangal, 506004, India

*Corresponding author. E-mail: sanil@student.nitw.ac.in

 SA, 0000-0002-4181-1366

ABSTRACT

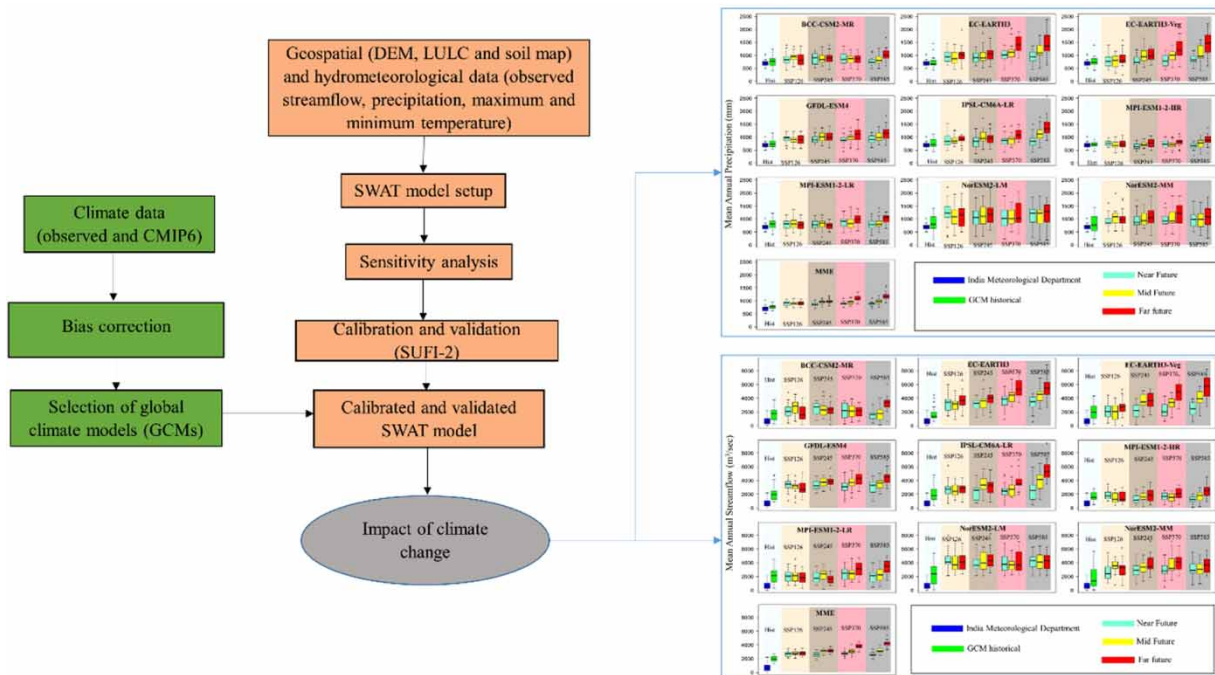
This study assessed the impacts of climate change on the water balance of the Krishna River Basin (KRB) in India. A frequency-based metric, known as symmetric uncertainty, was used to select the top 50% of global climate models (GCMs) from a pool of 18 Coupled Model Inter-comparison Project Phase 6 (CMIP6) GCMs for hydrological modelling. The impact of climate change was projected for three future time frames, namely, near future (NF: 2026–2050), mid-future (MF: 2051–2075) and far future (FF: 2076–2100), using four scenarios from shared socio-economic pathways (SSPs): SSP1-2.6, SSP2-4.5, SSP3-7.0, and SSP5-8.5. The Soil and Water Assessment Tool model was used to simulate climate change impact during historical and future periods in the basin. The results showed a significant increase in the annual average precipitation, surface runoff, water yield and streamflow in the future under all SSP scenarios. The increase in the projected annual average precipitation ranges from 12 to 54% for four SSP scenarios compared to the historical ensemble average. Future periods showed a shift in the monthly peak flows compared to the baseline period. More availability of water in the future in the KRB can be effectively used for various water management works.

Key words: climate change, CMIP6 scenarios, SWAT, symmetric uncertainty, water resources

HIGHLIGHTS

- The impact of climate change on the water balance of the Krishna River Basin was assessed using CMIP6-based climate models.
- The symmetric uncertainty concept was used to screen the 50% suitable GCMs from a pool of CMIP6 climate models.
- High values of NSE and R^2 at different gauging locations across the KRB suggested that the SWAT model is spatially performing well.
- The uncertainty bounds of simulated water balance components were estimated to understand the behaviour of selected GCMs.

GRAPHICAL ABSTRACT



1. INTRODUCTION

Climate change is one of the major challenges that must be addressed for sustainable development (Hang 2022). The changing climatic patterns and the increased frequency of extreme events are believed to have major impacts on human activities and ecological systems (IPCC 2013). Among various sectors, the water resources sector is expected to be severely affected by the changing climate. Climate change affects hydrological variables such as temperature and precipitation patterns, thereby altering the global hydrological cycle, which results in frequent floods and droughts (Murray *et al.* 2012; Zhang & Huang 2013; Faye 2022). The arid and semi-arid regions are most sensitive to climate change, especially to changes in the precipitation pattern (Gong *et al.* 2004; Vörösmarty *et al.* 2010; Xing & Wang 2017). Under the climate change scenarios, variations in streamflow have been found to be highly linked with precipitation changes. Quantification of the hydrological effects due to climate change is essential for better design and management of water resources of any region.

The future climate variable projections are obtained using the global climate models (GCMs), which are recognised as credible tools for simulating the long-term future climate in a changing environment (Srinivas *et al.* 2013; Gouda *et al.* 2018). Most climate change impact studies integrate the available GCM data into a hydrological model to analyse different scenarios. However, one of the shortcomings of this approach is the uncertainty associated with the predicted climate variables from different GCMs. One of the approaches to overcome this is analysing the climate change impacts using the outputs from multiple GCMs. While this method considers the uncertainty in the climate predictions, it leads to larger plausible impacts of climate change on the water balance components (WBCs). Some studies have reported that the performance of the GCM simulations is region-specific, possibly due to the resolution of the simulation, model structure, parameterisation and boundary conditions (IPCC 2013; McSweeney *et al.* 2015). Therefore, selecting the GCMs that best represent the climate of the study region is a pre-requisite for climate change studies, but it is seldom followed (Chiew *et al.* 2009; McMahon *et al.* 2015; Pour *et al.* 2018). Further, with the release of new climate change projections, ranking of GCMs for hydrological studies is required for analysing the impacts of climate change.

The evaluation of a climate model is typically conducted by comparing its simulation of historical data with a reference dataset. The evaluation of models was categorised into two groups: time-domain- and frequency-domain-based metrics, as discussed by Rathinasamy *et al.* (2014). The time-domain category metrics, such as coefficient of determination, Nash–Sutcliffe coefficient (NSE), root-mean-square error, fourth root-mean-square error, Kling–Gupta efficiency, etc., consolidate

the error at each time step into a singular metric. The majority of these metrics are highly susceptible to extreme events and outliers. The second category evaluates the similarity between the frequency distributions of observed and simulated variables to assess the goodness of fit. This overcomes previous limitations and allows a more comprehensive assessment of the match between observed and simulated data. Some of the studies used these frequency-domain metrics such as skill score (Perkins *et al.* 2007; Anandhi & Nanjundiah 2015; Raju *et al.* 2017) and Brier score (Ruan *et al.* 2018) in climate model selection. Symmetric uncertainty (SU) is one of the most used frequency-based metrics in recent studies for GCM selection (Khan *et al.* 2018; Hassan *et al.* 2020). The SU computes similarities and dissimilarities between simulated and observed time series in terms of common information entropies. The advantage of SU is that it does not depend on the distribution and conditional dependences of the data and can be used in place of conventional statistics (Khan *et al.* 2018; Salman *et al.* 2018). The present study used the SU technique to select suitable GCMs due to their advantage compared to other metrics.

Progressive efforts have been made to assess the impact of climate change on large river basins across the world using the outputs of different GCMs from Coupled Model Intercomparison Project (CMIP) Phases 3 and 5 (Githui *et al.* 2009; Chen *et al.* 2012; Gao *et al.* 2018; Reshmidevi *et al.* 2018; Bhatta *et al.* 2019; Ndhlovu & Woyessa 2020; Mann & Gupta 2022). The results of these studies indicate that the changes in climatic patterns and their impacts on the hydrology of watersheds vary with location and catchments in addition to climate models and their projection scenarios. The water yield increased in some basins, while it decreased in other basins. Indian river basins (IRBs) are exceptionally susceptible to extreme events such as floods and droughts (Suman & Maity 2020; Poonia & Azad 2022). In the context of IRBs, Reshmidevi *et al.* (2018) used an ensemble of CMIP3-based GCMs under the A2 scenario to investigate the impact of climate change on the Malaprabha River Basin and observed that marginal changes occurred in annual future precipitation and insignificant changes happened in the future water budget components. In another study, Pandey *et al.* (2019) investigated the effect of climate change on the Narmada River Basin using CMIP5 projections and found a significant decrease in the annual precipitation in the future under both representative concentration pathway (RCP)4.5 and RCP8.5 scenarios. They also observed that other WBCs were also significantly affected.

The Krishna River Basin (KRB) is one of the major river basins in India and a fast-developing region in the Indian peninsula. The water needs in the KRB are increasing day by day for agriculture, domestic and industrial purposes due to the rapid increase in population and economic growth, which may lead to water shortage and interstate conflict in the future. A study estimates that the water demand is more than the supply in half of the KRB (Lower Krishna, Paleru, Vedavathi, Munneru, Musi and Middle Krishna) (Yee *et al.* 2009). In addition, the KRB is highly sensitive to climate variations due to its semi-arid nature, which may affect water demand, especially in the agricultural sector (Yee *et al.* 2009). Therefore, analysing the climate change impacts on the KRB for developing prudent water management strategies is essential. Only a few studies are available that evaluate the climate change impacts on the water resources of the KRB. For instance, it is predicted that the decrease in the precipitation and water yield will lead to seasonal or regular water stress and drought conditions in the future under greenhouse gas (GHG) scenarios and special report on emission scenarios (SRES) (Gosain *et al.* 2006, 2011). Kulkarni *et al.* (2014) predicted an increase in annual precipitation, water yield, surface runoff, and actual evapotranspiration for the future period of 2041–2070 under the SRES. However, they found no notable variations in these parameters during the early century (2011–2040). The study did not consider the water storage structures, and it utilised data from a single GCM without any bias correction and performed calibration at only one gauge station. However, the aforementioned studies rely on utilising GHG and SRES, which inherently contain significant uncertainties due to assumptions made regarding economic development, population growth and technological advancements (Soro *et al.* 2017). In another study on KRB, an increase in the discharge and hydrological extremes in the future under RCP4.5 and RCP8.5 scenarios using only a single regional climate model IITMRegCM4-4 was observed (Nikam *et al.* 2018). Similarly, the increasing trend of WBC is projected in some of the studies under CMIP5 projections within RCP4.5 and RCP8.5 scenarios using randomly selected GCMs (Mishra & Lilhare 2016; Chanapathi *et al.* 2018). Considering water storage structures in hydrological modelling will also improve the accuracy of the future projections of WBCs. Relying on a single GCM or random selection of GCMs may incorporate large uncertainty in climate change studies. Hence, the simulations of the multi-model ensemble (MME) mean are identified as a better estimate (Gleckler *et al.* 2008; Knutti *et al.* 2010). It is suggested that 50% of top-performing GCMs are optimum for the climate change impact studies to reduce the uncertainty in the model projections (Ahmed *et al.* 2020; Raju & Nagesh Kumar 2020). However, at present, CMIP6 comprises a more complex atmospheric process and has an improvised parameterisation that can efficiently simulate model ability (Eyring *et al.* 2016; O'Neill *et al.* 2016). It is reported that CMIP6 GCMs are more efficient in simulating the Indian summer monsoon than CMIP5 GCMs (Gusain *et al.* 2020). The

climate change impact studies using an improved version of the CMIP5 project, i.e., the CMIP6 climate model, are lacking in the KRB. Therefore, the objectives of the present study are (i) to evaluate the performance of climate models to identify the most suitable GCMs from CMIP6 using the SU concept for KRB, (ii) to assess the impact of projected climate change on WBCs including streamflow using the SWAT model for different bias-corrected socio-economic pathways (SSPs) scenarios and (iii) to analyse the streamflow extremes in KRB.

2. STUDY AREA AND DATA

2.1. Study area

The KRB is the fifth largest river basin in India. It covers a geographical area of about 258,948 km² (8% of the country) and extends between 13°5′–19°24′N latitude and 73°20′–81°E longitude, as shown in Figure 1. The river originates from the Mahadev range of Western Ghats in Maharashtra state and flows approximately 1,400 km, covering Maharashtra, Karnataka, Telangana and Andhra Pradesh states, and finally drains into the Bay of Bengal. It is mainly divided into seven sub-basins by the Central Water Commission (CWC), namely, Upper and Lower Bhima; Upper, Middle and Lower Krishna and Upper and Lower Tungabhadra.

The basin's climate varies from humid to arid, where most parts (inland areas) fall under semi-arid nature. Approximately 80% of the basin is composed of Archaean and crystalline rocks, with the remaining 20% comprising basalts (Ramesh & Subramanian 1988); additionally, laterite and black soils are prevalent in the area (Das *et al.* 2005). The land use/land cover is dominated by agriculture, which covers nearly 76% of the area. Average annual rainfall varies from 429 mm in the northern part to 3,080 mm in the southern part, with an average of 745 mm. Average daily maximum and minimum temperatures vary from 27.7 to 40.4 °C and from 20.6 to 27.2 °C, respectively. The southwest monsoon (June–September) period has the predominant rainfall distribution (nearly 90%). The uneven distribution of rainfall occurring in the basin affects the

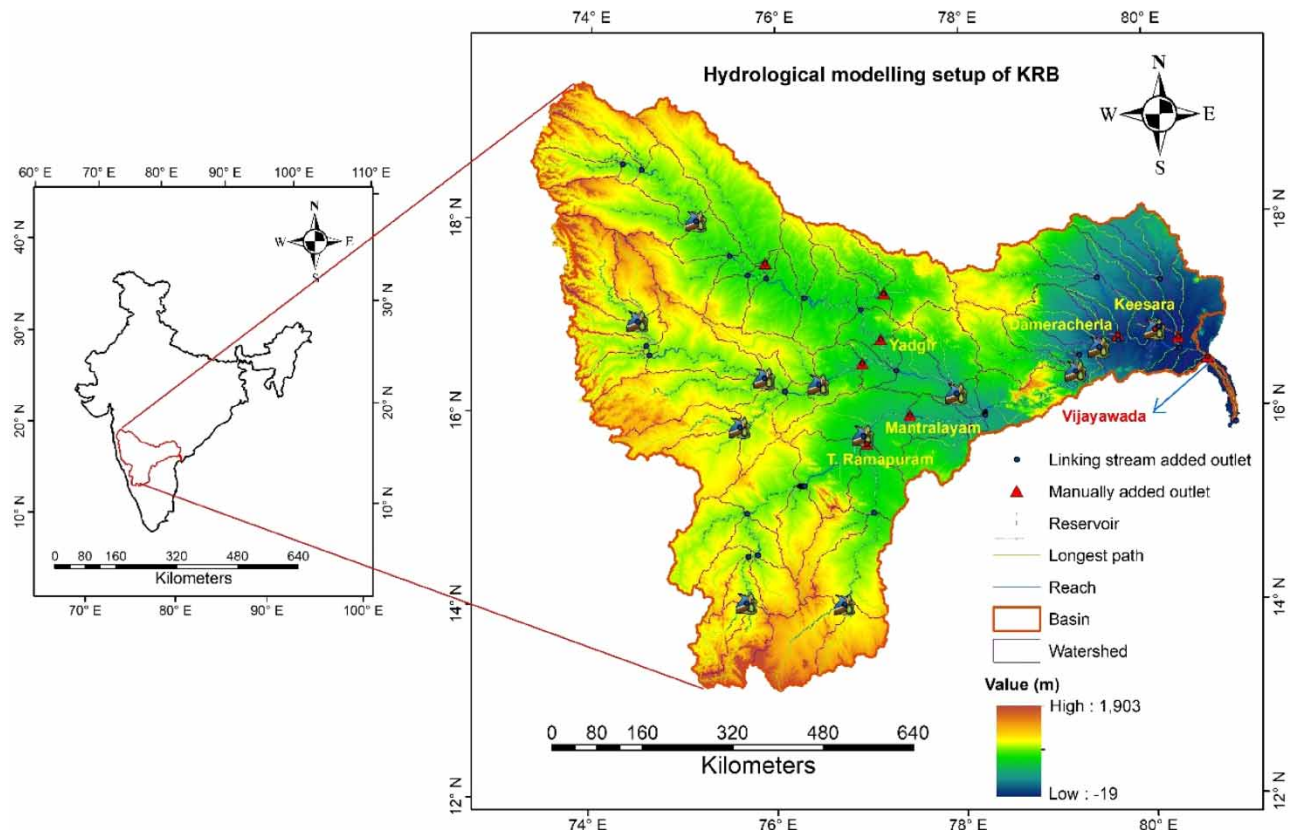


Figure 1 | Geographical location and model set-up with reservoirs considered in KRB.

availability of water. Some parts of the basin experience droughts (Singh *et al.* 2019), whereas delta regions are prone to flooding (<http://india-wris.nrsc.gov.in>).

2.2. Data

Datasets necessary for setting up the soil and water assessment tool (SWAT) hydrological model included spatial data such as the digital elevation model (DEM), land use land cover (LULC) maps, soil maps and meteorological information, including precipitation levels and minimum and maximum temperatures. The discharge at multiple locations within the basin was used to calibrate the SWAT model.

2.2.1. Spatial data

A 30 m resolution of DEM available from the Shuttle Radar Topography Mission was used to delineate KRB (<http://dwtkns.com/srtm30m/>). The required LULC was taken from the water base (<http://www.waterbase.org/>), and the digital soil map was taken from the Food and Agriculture Organization, with a scale of 1:5,000,000. All these spatial maps represent the heterogeneity of the catchment and are converted into the required projected coordinate system (Figure 2).

2.2.2. Hydrometeorological data

In India, the hydrometeorological stations are maintained by the CWC. Daily discharge data observed at the Vijayawada gauging station (mouth of KRB) from 1970 to 2003 and information regarding monthly storage, volume, area, effective and gross storage capacity of the hydraulic structures, and spillway designed capacities were downloaded from the Water Resources Information System (India-WRIS) (<https://indiawris.gov.in/wris/>). Daily gridded precipitation of $0.25^\circ \times 0.25^\circ$ and minimum and maximum temperatures of $0.5^\circ \times 0.5^\circ$ were obtained from the Indian Metrological Department (IMD; <https://www.imdpune.gov.in/>). The precipitation dataset had no missing values and was developed from 6,955 gauging stations distributed all over India (Pai *et al.* 2014). These data performed better than other global gridded datasets such as the National Centers

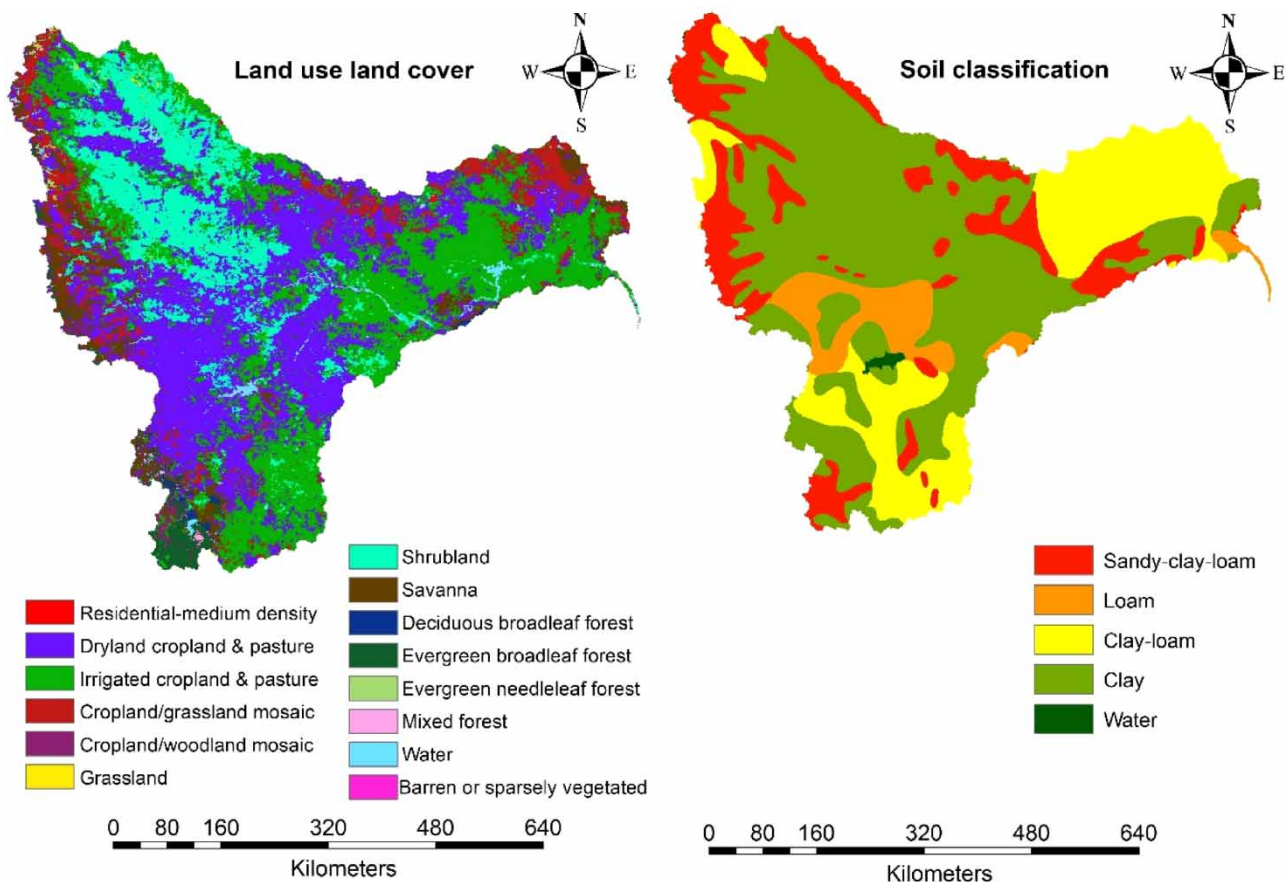


Figure 2 | LULC and soil maps of the KRB.

for Environmental Prediction, Coordinated Regional Climate Downscaling Experiment, and Global Precipitation Climatology Project (Bandyopadhyay *et al.* 2018).

2.2.3. GCM data

Daily precipitation data from GCMs of CMIP6 repositories were considered in this study. This study used scenarios from Tier-1 Shared Socio-economic Pathways (SSPs) that include SSP1-2.6, SSP2-4.5, SSP3-7.0 and SSP5-8.5 to provide a full range of forcing targets similar in both magnitude and distribution to the RCPs used in CMIP5 (Gidden *et al.* 2019), as presented in Table 1. The GCM data can be accessed from the Earth System Grid Federation portal (<https://esgf-node.llnl.gov/search/cmip6>).

3. METHODOLOGY

The future climate change impact on the hydrology of KRB is categorised into four phases: (1) selection of the suitable GCMs from CMIP6, (2) SWAT model setup and performance evaluation using calibration and validation, (3) future climate change assessment based on WBCs and (4) analysis of streamflow extremes in the KRB.

3.1. GCMs ranking

Selection of suitable GCMs for a given study is necessary to reduce uncertainty induced in the GCMs. Initially, 18 GCM precipitation outputs were considered from the first ensemble member ('r1i1p1f1') experiment family and re-gridded to the observed data resolution of $0.25^\circ \times 0.25^\circ$ using the bilinear interpolation technique (Pour *et al.* 2018; Anil *et al.* 2021). Due to the presence of biases in the GCMs, their projections are often unreliable. Many studies have used various bias correction methods to reduce biases (Eisner *et al.* 2012; Pierce *et al.* 2015; Maraun *et al.* 2017). In this study, empirical quantile mapping, one of the most useful and robust non-parametric techniques, was employed to reduce the biases associated with the historical and future scenarios of GCM outputs (Piani *et al.* 2010; Mishra *et al.* 2020).

The widely used concept called SU (Homsy *et al.* 2020) was applied to precipitation for the 1951–2014 period to screen the suitable GCMs. The SU was computed based on mutual information (MI) to find similarities and dissimilarities between simulated and observed time series in terms of common information entropies. MI tends to be biased towards higher values, and

Table 1 | List of GCMs considered in the present study

Serial no.	GCM name	Developed by	Resolution (long. \times lat.)
1	ACCESS-CM2	Australia	$1.875^\circ \times 1.25^\circ$
2	ACCESS-ESM1-5	Australia	$1.875^\circ \times 1.25^\circ$
3	BCC_CSM2-MR	China	$1.13^\circ \times 1.12^\circ$
4	CanESM5	Canada	$2.81^\circ \times 2.79^\circ$
5	CESM2-WACCM	USA	$1.25^\circ \times 0.94^\circ$
6	EC-EARTH3	Netherlands/Ireland	$0.7^\circ \times 0.7^\circ$
7	EC-EARTH3-Veg	Netherlands/Ireland	$0.7^\circ \times 0.7^\circ$
8	GFDL-ESM4	USA	$1.25^\circ \times 1^\circ$
9	IITM	India	$1.88^\circ \times 1.88^\circ$
10	INM-CM4-8	Russia	$2^\circ \times 1.5^\circ$
11	INM-CM5-0	Russia	$2^\circ \times 1.5^\circ$
12	IPSL-CM6A-LR	France	$2.5^\circ \times 1.27^\circ$
13	MIROC6	Japan	$1.4^\circ \times 1.4^\circ$
14	MPI-ESM1-2-HR	Germany	$0.94^\circ \times 0.94^\circ$
15	MPI-ESM1-2-LR	Germany	$1.88^\circ \times 1.85^\circ$
16	MRI-ESM2-0	Japan	$1.13^\circ \times 1.12^\circ$
17	NorESM2-LM	Norway	$2.5^\circ \times 1.89^\circ$
18	NorESM2-MM	Norway	$1.25^\circ \times 0.94^\circ$

this bias can be mitigated using SU by normalising the MI in the range of 0–1 (Salman *et al.* 2018). An SU value of 1 indicates perfect agreement, while a value of 0 indicates no agreement between the observed and simulated time series. It has been reported that there is no rule for selecting the number of GCMs, and most have considered the top three to five GCMs (Tian *et al.* 2016; Wang *et al.* 2016; Latif *et al.* 2018; Ahmed *et al.* 2019; Noor *et al.* 2019; Shiru *et al.* 2019; Iqbal *et al.* 2020) to develop MME average to reduce the uncertainty. However, some studies have reported that the optimum performance of MME is achieved when 50% of the top-ranked GCMs are considered (Ahmed *et al.* 2020; Raju & Nagesh Kumar 2020). In the present study, nine GCMs are selected for further climate impact studies based on the total ranking weight (TRW) obtained using Equation (1) after applying SU. The following steps are involved in the ranking of GCMs:

- (i) By using the SU score, GCMs are ranked first, second, third, and so on at each grid point.
- (ii) Weights (w_i) are assigned to each GCM in such a way that their ranking is inversely proportional.
- (iii) For each rank, the frequency (Fr_i) of each GCM is calculated. Finally, the total ranking weight of each GCM is computed using the following equation:

$$\left(\text{TRW} = \sum_{i=1}^5 Fr_i * w_i \right) \quad (1)$$

After sorting the TRW in descending order, the GCM's final ranking is determined. For a detailed explanation regarding the concept of SU and the procedure involved in selecting the ranking of GCMs, readers can refer to Anil & Anand Raj (2022).

3.2. SWAT model

The SWAT model can simulate the impacts of the long-term climate and LULC variations on the hydrology in large complex catchments (Wang *et al.* 2008; Neitsch *et al.* 2011; Arnold *et al.* 2012). The SWAT model divides the entire catchment into sub-catchments based on topography and then segregates these sub-catchments into hydrological response units (HRUs) using the unique combinations of slope, LULC and soil classes. The HRUs are vertically divided into different control volumes like surface layer, root zone, shallow aquifer and deep aquifer. Using climate data and LULC patterns, the SWAT model can estimate anticipated watershed scenarios. Moreover, it can evaluate streamflow variability by taking into account forecasted climate variables for the future.

3.2.1. SWAT model set-up

The entire KRB was divided into 85 sub-basins after the delineation process, and a 5% overlap of LULC, soil and slope was provided to define HRUs, resulting in 1,490 HRUs. The water storage structures in any basin will significantly influence the performance of the model, which shows an impact on the WBC (Sahoo *et al.* 2018; Chanapathi & Thatikonda 2020). To improve the model performance and reduce the uncertainty in the output, 13 major reservoirs—Bhadra, Tungabhadra, Nagarjunasagar, Srisailem, Almatti, Koyana, Narayanapura, P.D. Jurala, Ujjaini, Malaprabha, Pulichintala, Hidkal and Vaanivilas—were considered based on the data availability from CWC for setting up the model. Various details of reservoirs are provided, such as area, volume, principal, gross storage, live capacity, principle volume, emergency, principle surface area, design flood, maximum and minimum monthly outflows, target storage capacity and consumptive storage capacity. Observed data for 34 years (1970–2003) were considered for calibrating and validating the SWAT model. The first 3-year (1970–1972) data were taken as a warm-up period.

The SWAT model was calibrated and validated using the sequential uncertainty fitting (SUFI-2) algorithm in the SWAT-Calibration and Uncertainty Program (CUP) (Abbaspour *et al.* 2015). Prior to calibration, the sensitivity of the model parameters influencing streamflow was estimated in the SWAT-CUP. The p -values and t -test values were used to identify the sensitive parameters that can influence the model output. Smaller p -values with larger t -test values represent higher sensitivity for the optimisation function and thus the observed variable, i.e., discharge. The t -test represents the relative significance, while the p -value represents the significance of sensitivity (Sinha *et al.* 2020).

4. RESULTS AND DISCUSSION

4.1. Climate model selection

The SU technique was employed to choose the top nine GCMs to reduce the uncertainty in climate model projections. The TRW of the 18 considered GCMs is shown in Figure 3. As mentioned previously, the performance of the GCMs was evaluated

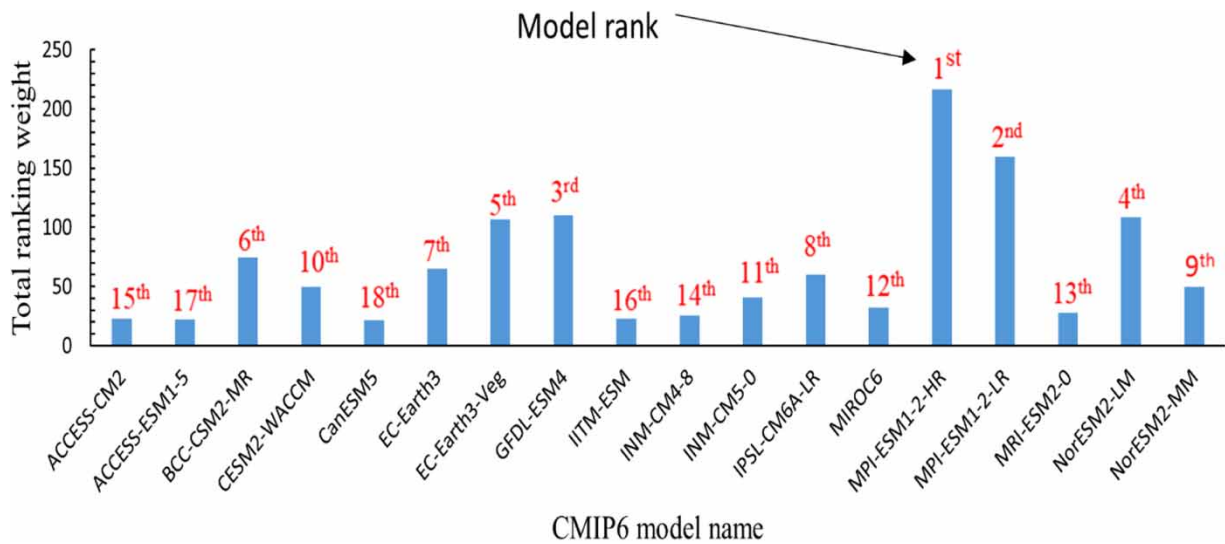


Figure 3 | Ranking of each GCM-based total ranking weight (TRW).

in all 348 grids within the KRB. The spatial distribution of the best-performing GCMs from rank 1 to rank 5 is shown in Figure 4. For the first rank, GCM MPI-ESM1-2HR exhibited the best performance in 50% of the grids, i.e., 165 in terms of the SU value. The output of MPI-ESM1-2-LR was observed to be best in 60 grid points and was ranked 2. Similarly, EC-Earth3, NorESM2-LM and GFDL-ESM4 secured ranks 3, 4 and 5, respectively, in terms of the maximum numbers of grids from a single GCM. From Figure 4, it is evident that as the rank of the GCM increased, the performance of different GCMs appeared comparable, resulting in wide variations. The ranking of each GCM was computed based on the frequency

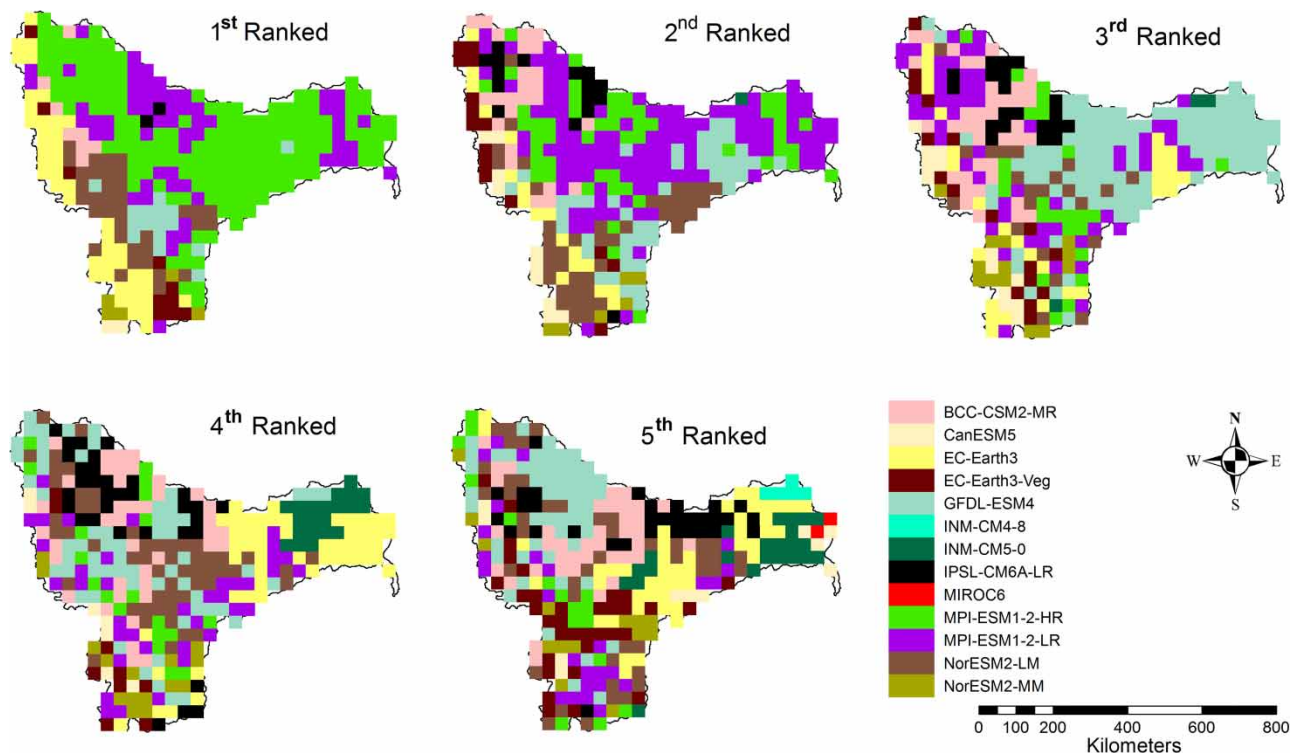


Figure 4 | Spatial distribution of the top-ranked GCMs.

of occurrence of each GCM from rank 1 to rank 5 and was computed as the TRW. Based on the results, the top nine suitable GCMs, namely, MPI-ESM1-2-HR, MPI-ESM1-2-LR, GFDL-ESM4, NorESM2-LM, EC-Earth3-Veg, BCC-CSM2-MR, EC-Earth3, IPSL-CM6A-LR and NorESM2-MM, were considered for further analysis.

4.2. SWAT model performance evaluation

The SWAT model was calibrated and validated monthly using the observed discharge at six outlet stations. The sub-basin discretisation for the SWAT model, along with the locations of reservoirs and gauge points, is shown in Figure 1. The model was simulated from 1970 to 2003, with the first 3 years considered a warm-up period. The calibration of the model was performed for 21 years, i.e., 1973–1993, and validation was performed for 10 years, i.e., 1994–2003, using the SUFI-2 algorithm in the SWAT-CUP. Based on previous studies, 12 parameters that influenced the streamflow were selected for the calibration (Table 2). Among these parameters, nine, i.e., CN2, GWQMN, ESCO, SOL_AWC, CH_N2, REVAPMN, GW_DELAY, CH_K2 and GW_REVAP, were identified as the most sensitive parameters after 500 iterations (Fig. S1, Supplementary material). The performance of the model during calibration and validation was assessed using the NSE and the coefficient of determination (R^2). A similar R^2 and NSE value of 0.79 was obtained during the calibration period, which is considered good as per the suggestions given by Moriasi *et al.* (2015). For the validation period, the R^2 and NSE values of 0.65 and 0.64 were obtained, respectively, which is considered satisfactory. The model demonstrates good performance during the calibration and validation periods, evident in the close assignment between the simulated and observed hydrographs, as shown in Figure 5. The performance of the model was also compared using other statistical performance measures such as PBIAS, p -factor and r -factor, as presented in Table 3. The p -factor represents the percentage of observed data enclosed within the 95PPU and ranges from 0 to 1. For the streamflow, a p -factor value of >0.7 is considered good. The r -factor indicates the width of the 95PPU band, and a value of <1.5 is considered desirable. In the present study, the p -factor and r -factor values at the Vijayawada gauging station were observed as 0.62 and 1.06, respectively, and were considered satisfactory (Abbaspour *et al.* 2015). The negative values of the PBIAS in both calibration and validation periods indicate that the model has underpredicted the streamflow compared to the observed flow. The calibrated and validated model was also evaluated at other gauging locations, as presented in Table 4 and Figure 6. The high values of NSE, R^2 and PBIAS at different gauging locations across the KRB suggest that the model is spatially performing well. The good performance of the calibrated model suggests that the model can capture the spatial and temporal variability of the hydrological processes properly within the basin.

4.3. Climate change impact on WBC in the KRB

The impact of climate change on the hydrology of the KRB was assessed using the selected nine GCMs for the four scenarios of SSP1-2.6, SSP2-4.5, SSP3-7.0 and SSP5-8.5. The analysis was performed for three future time periods, i.e., near future

Table 2 | Calibrated parameters of the SWAT model

Parameter	Definition	Range	Fitted value
r_CN2.mgt	Soil Conservation Service runoff curve number	–0.1 to 0.1	–0.0946
v_ALPHA_BF.gw	Base flow alpha factor (days)	0.2–0.8	0.7526
a_GW_DELAY.gw	Groundwater delay time (days)	–30 to 90	–21.960001
a_GWQMN.gw	Threshold depth of water in the shallow aquifer required for return flow to occur (mm)	–1,000 to 1,000	250
r_SOL_AWC().sol	Available water capacity of the soil layer (mm/mm)	–0.1 to 0.1	–0.009
a_REVAPMN.gw	Threshold depth of water in the shallow aquifer for ‘revap’ to occur (mm)	–750 to 750	–154.5
a_RCHRG_DP.gw	Deep aquifer percolation coefficient	–0.05 to 0.05	0.0175
v_GW_REVAP.gw	Groundwater ‘revap’ coefficient	0.02–0.2	0.0569
v_CH_N2.rte	Manning’s n value for the main channel	0–0.2	0.0146
v_CH_K2.rte	Effective hydraulic conductivity in main channel alluvium (mm/h)	0–100	81.900002
r_OV_N.hru	Manning’s n value for overland flow	–0.2 to 0.2	0.1532
v_ESCO.hru	Soil evaporation compensation factor	0–0.8	0.1576

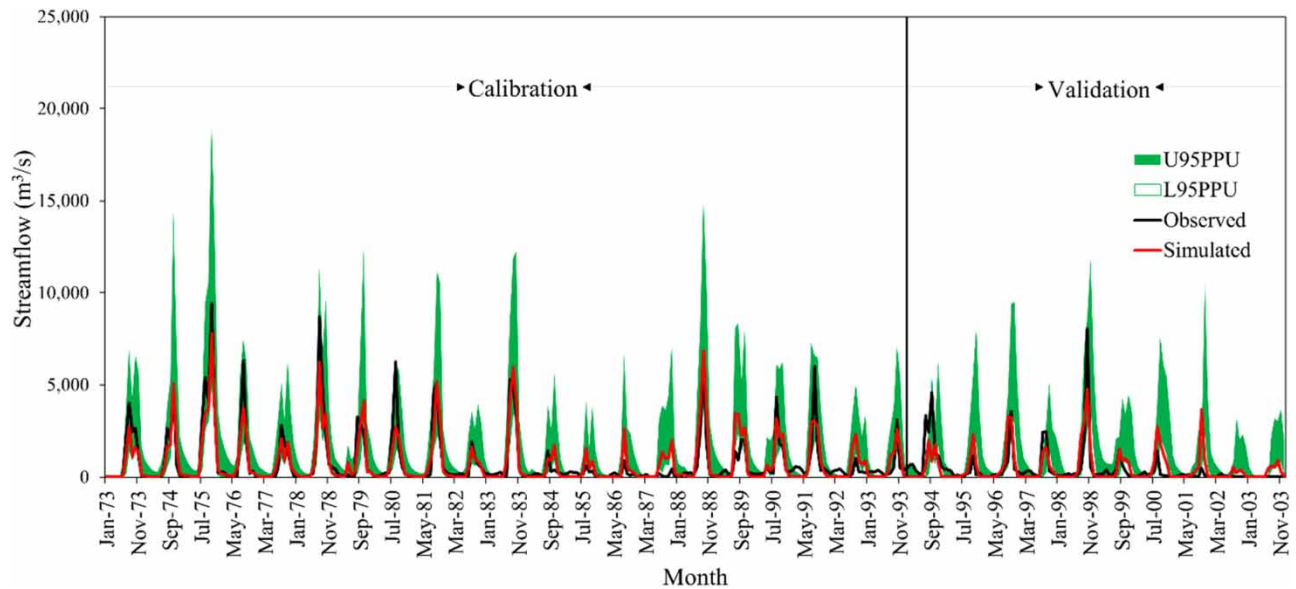


Figure 5 | Depiction of simulated and observed streamflow for calibration and validation periods.

Table 3 | Performance evaluation values for calibration and validation at the Vijayawada gauging station

Parameter	Calibration	Validation
NSE	0.79	0.65
R^2	0.79	0.64
PBIAS	-0.9	-11.5
p -factor	0.62	0.57
r -factor	1.06	1.29

Table 4 | Performance evaluation values for calibration and validation at different stations

Sub-basin (station no.)	Calibration		Validation		PBIAS	p -factor	r -factor
	R^2	NSE	R^2	NSE			
Mantralayam (66)	0.80	0.78	0.70	0.68	16.8	0.63	0.88
T.Ramapuram (72)	0.67	0.57	0.65	0.58	16.3	0.73	1.37
Yadagir (33)	0.78	0.77	0.67	0.67	6.8	0.8	0.82
Keesara (32)	0.86	0.84	0.61	0.58	2.7	0.77	1.10
Dameracherla (29)	0.54	0.53	0.63	0.45	9.2	0.65	1.9

(NF: 2026-2050), mid-future (MF: 2051-2075) and far future (FF: 2076-2100). This study assessed the impact of climate change on the WBCs, i.e., precipitation, evapotranspiration, surface runoff, water yield and streamflow at the watershed outlet. Historical simulations for each of the GCMs were input into the SWAT model to obtain the historical output, which served as the baseline for assessing the impact of climate change associated with each GCM (Figures 7–10). A comparison was also made between the WBC simulations obtained from historical GCM and the observed IMD data for the baseline period, i.e., 1973–2003. The uncertainty in the future projections is evident from the difference in the projected values from different GCMs, as shown in Figures 7–10. During the baseline period 1973–2003, the average annual precipitation projections for the historical GCMs ranged from 713 to 796 mm, compared to the observed precipitation value of 697 mm. Among the nine GCMs, MPI-

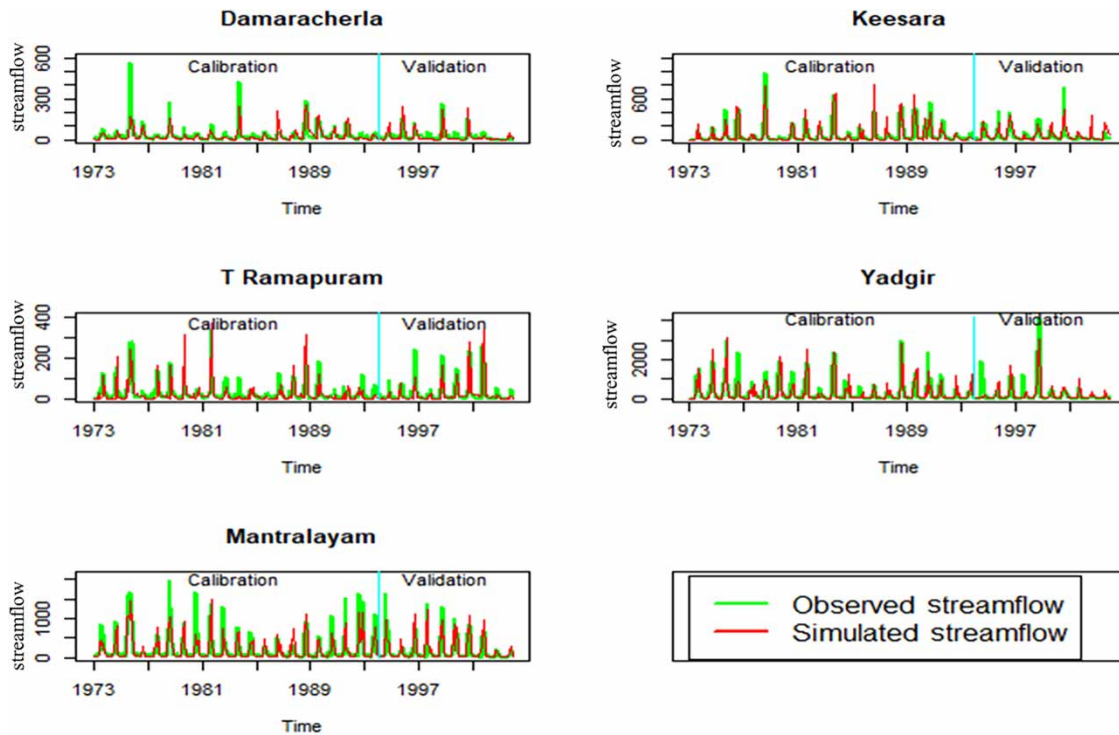


Figure 6 | Depiction of simulated and observed streamflow for calibration and validation periods at different gauging stations.

ESM1-2-HR, EC-EARTH3 and EC-EARTH3-Veg models displayed less deviation from observed precipitation during the baseline period, whereas NorESM2-LM and NorESM2-MM models exhibited maximum variation compared to other GCMs (see Figure 7). The future precipitation projections for four SSP scenarios exhibited a significant increase for each GCM compared to the historical GCM, except for MPI-ESM1-2-HR and MPI-ESM1-2-LR. Compared to the historical period, the EC-EARTH3 and EC-EARTH3-Veg models showed the highest range in projected precipitation change under all SSP scenarios. It was also observed that future precipitation increases from NF to FF under all scenarios for all GCMs. To understand the variation of precipitation for each GCM, the annual average precipitation changes of the historical period for each GCM with respect to observed IMD data were analysed and are provided in the supplementary material as Table S1. Similarly, the percentage changes in the projections of precipitation of each GCM with respect to the same GCM in the future are provided in the supplementary material as Table S2. The variation in projections of the annual average precipitation compared to historical GCMs are in the range of -5.7% for MPI-ESM1-2-LR to 100.9% for EC-EARTH3 in the future under SSP2-4.5 and SSP5-8.5, respectively. NorESM2-LM and NorESM2-MM models project more precipitation in the future compared to other historical GCM projections under all SSP scenarios except SSP5-8.5 in the FF. In the FF, the EC-EARTH3-Veg model projected the highest precipitation compared to that in the historical period. The surface runoff and water yield components also follow similar increasing patterns to the precipitation under all GCMs in the historical period. The annual MME averages of surface runoff and water yield are projected to increase up to 92 and 127%, respectively, compared to those in the historical period. The significant increase in water yield and surface runoff has led to a corresponding increase in streamflow across all GCMs. Comparisons of surface runoff, water yield and streamflow between each GCM for the future periods under four SSP scenarios are provided in the supplementary material as Tables S3–S5, respectively.

A comparison of the future projected precipitation from all GCMs with the historical GCM observed precipitation indicates that the mean precipitation in the basin is increasing in most future scenarios. Only a few years in all the GCM simulations have shown lower precipitation than the historical GCM precipitation within the basin. It is also observed that the variability in the future projected mean annual precipitation is increasing, as evident from the box plots of Figure 7. The MPI-ESM1-2-HR and MPI-ESM1-2-LR GCMs, which occupied first and second ranks in GCM ranking, predicted less increment in the future compared to other GCMs. It can be seen that NorESM2-LM and NorESM2-MM overestimated the higher extremes and underestimated the lower extremes. Although NorESM2-LM ranked fourth in GCM ranking, it

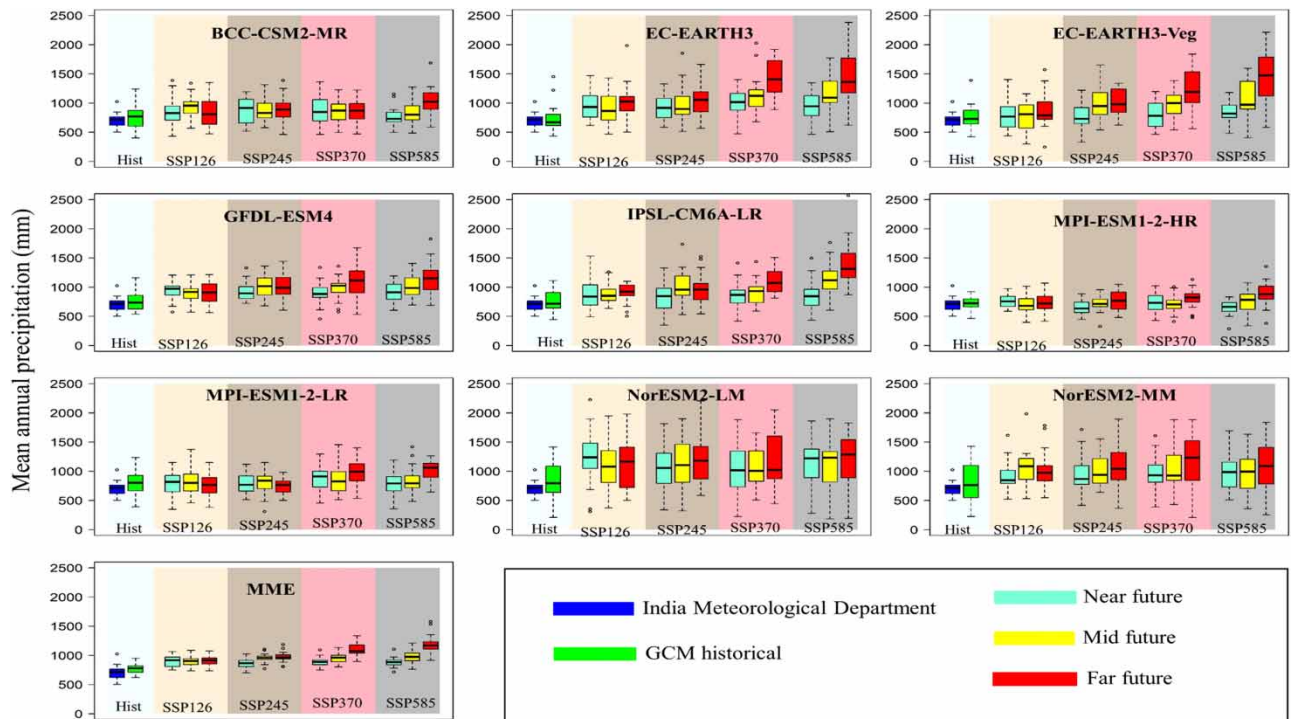


Figure 7 | Average annual precipitation under different SSP scenarios compared to observed IMD data.

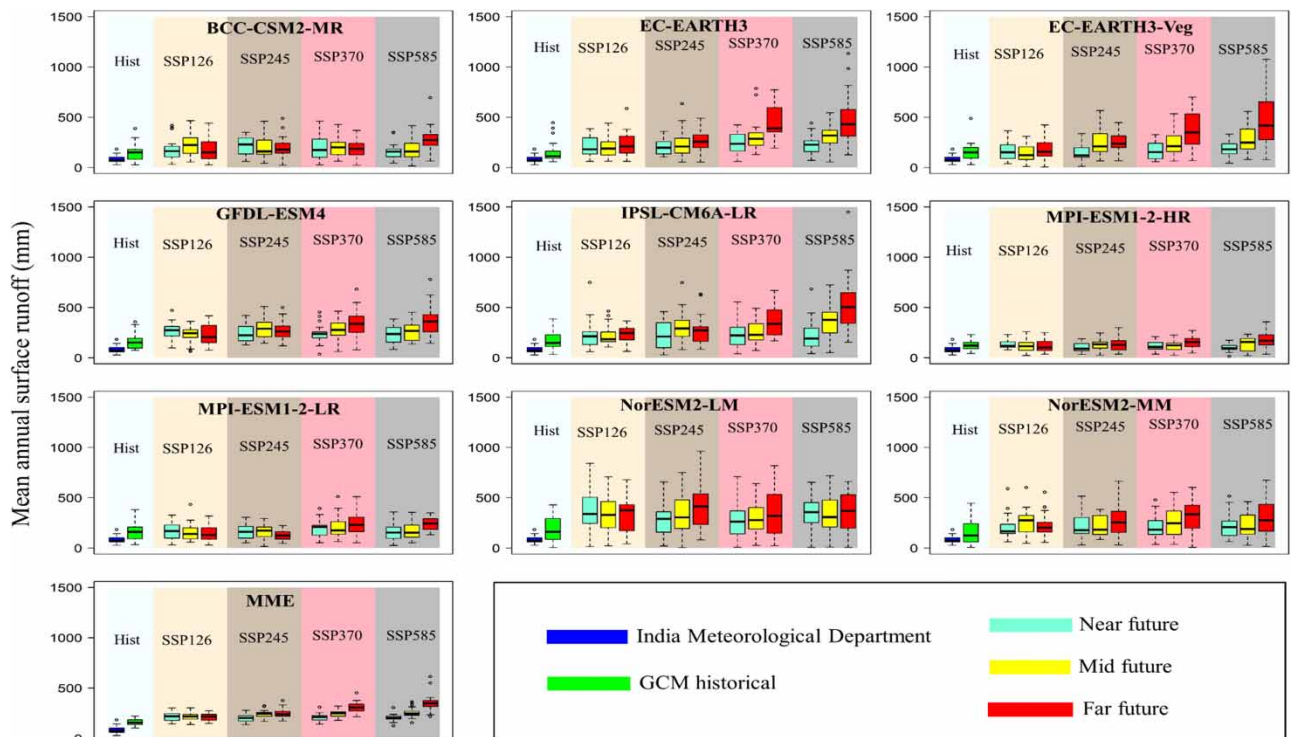


Figure 8 | Average annual surface runoff under different SSP scenarios compared to observed IMD data.

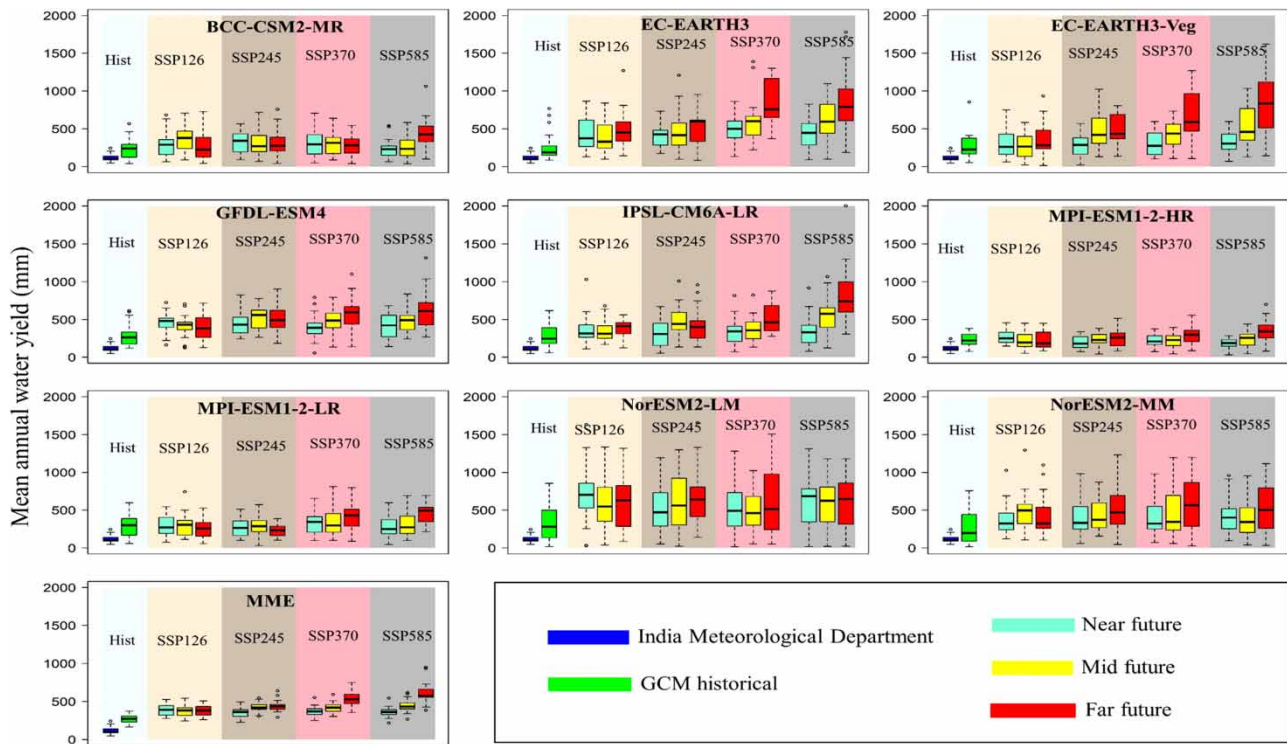


Figure 9 | Average annual water yield under different SSP scenarios compared to observed IMD data.

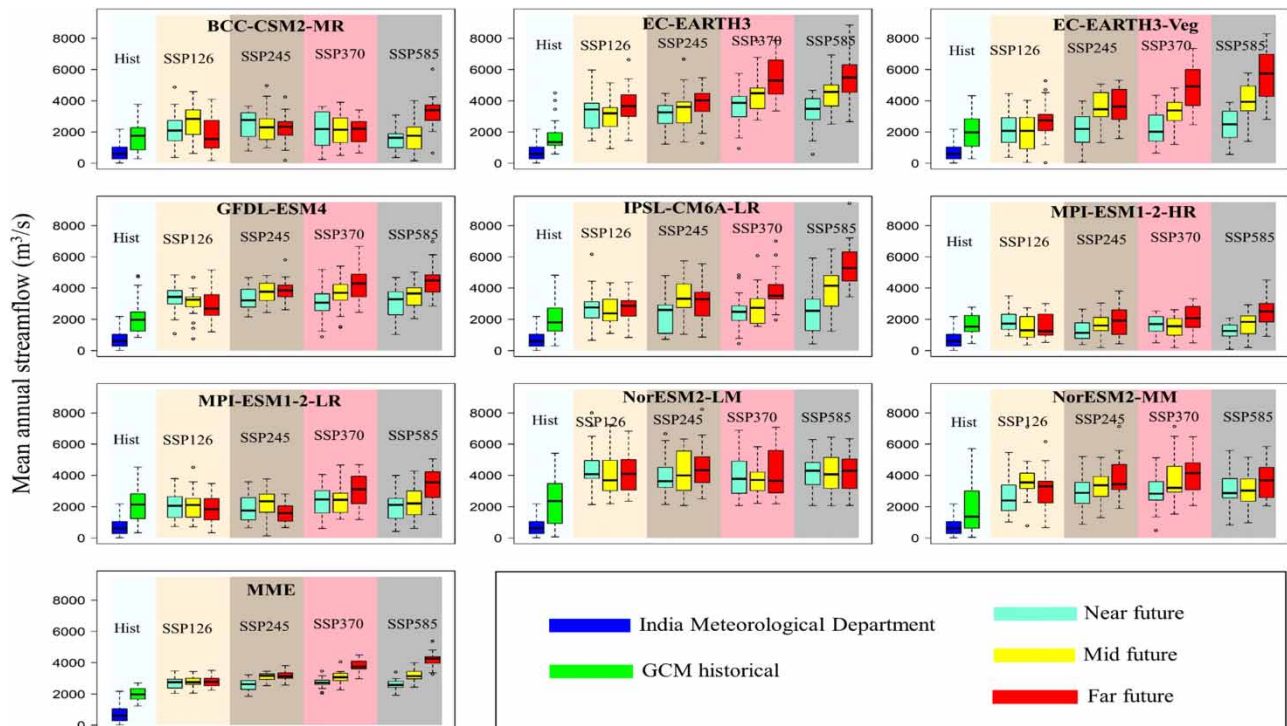


Figure 10 | Average annual streamflow under different SSP scenarios compared to observed IMD data.

showed more extremes compared to other GCMs in all periods except FF under SSP5-8.5. This could be due to the inherent fundamental uncertainties in the climate change projection of GCMs (Li & Jin 2017; Ndhlovu & Woyessa 2020). The Ec-Earth3 and Ec-Earth3-Veg outputs predicted more precipitation in FF under SSP5-8.5. In the FF, the precipitation magnitude increase was more than that in the NF and MF under SSP3-7.0 and SSP5-8.5. The high variability in the precipitation for the future projected GCMs suggests that the basin will experience climate extremes more frequently in the future. The increase in the total projected precipitation is also evident from the MME average value for the three future periods. The prediction bounds and percentage changes in the future projections are evident from the difference in the projected values from different GCMs (see Tables S6 and S7, Supplementary material). The ensemble mean of projected annual precipitation is projected to increase by 24.1–70.3% in future time frames compared to the observed IMD data in the baseline period. The maximum average annual precipitation is predicted to increase by 30.56, 39.31, 56.96 and 70.30% by the end of the 21st century under SSP1-2.6, SSP2-4.5, SSP3-7.0 and SSP5-8.5, respectively, compared to the observed IMD data in the baseline period.

The increased precipitation in the historical GCMs compared to the observed data is translated to other WBCs such as water yield, surface runoff and streamflow at the catchment outlet. Similarly, the future scenarios of all GCMs are also following a similar increasing trend in WBC to that of historical GCMs. Water yield, surface runoff and streamflow showed an increase in years with increasing rainfall, while in some years, these values were lower than the historical GCM. The increase in the surface runoff, water yield and streamflow at the outlet follows a similar trend to the precipitation data. Precipitation change has a significant influence on future streamflow, with projections showing a potential increase of 31–114.5% (see Tables S6 and S7, Supplementary material). The maximum ensemble mean changes in average annual streamflow are projected to increase 40.5, 61, 91 and 114.5% under SSP1-2.6, SSP2-4.5, SSP3-7.0 and SSP5-8.5, respectively, compared to the historical GCM ensemble average of the baseline period by the end of the 21st century. The variation of mean annual future streamflow shows significantly increasing trends from NF to FF under all SSPs (Figure 10) compared to the baseline period of historical GCMs. Among the four SSP scenarios, the highest increase in projected streamflow is projected to occur under SSP3-7.0 and SSP5-8.5 compared to the historical GCM streamflow of the baseline period. In the NF and MF, NorESM1-2-LM is predicting more future streamflow under SSP1-2.6 and SSP2-4.5. For the scenarios of SSP3-7.0 and SSP5-8.5, the maximum average streamflow values are observed for EC-EARTH3 output during the MF. The FF is experiencing higher magnitudes of streamflow, especially under the SSP5-8.5 scenario, compared to other periods. It is also observed that a maximum flow of 8,856 m³/s has occurred in the FF under the SSP5-8.5 scenario for EC-EARTH3 GCM output, which is 1.96 times the maximum flow value (4,500 m³/s) of the GCM historical. In contrast, the peak flow of the ensemble average is predicted in the future as 5,381 m³/s, which is two times the peak flow (2,692.7 m³/s) of the ensemble average during the baseline period. The highest precipitation, water yield, surface runoff and streamflow are projected to increase by 54, 125, 124 and 114.5%, respectively, in FF under the SSP5-8.5 scenario compared to the ensemble average of the baseline period. The higher increase in the water yield, surface runoff and streamflow components compared to the precipitation may suggest that the level of precipitation is increasing during the monsoon period, leading to saturated conditions, which could result in higher runoff generation. The percentage increase in the evapotranspiration (ET) is observed to be, in general, low for future periods compared to the other WBCs (see Table S7). The ET is projected to increase in the range of 4–18% for future periods under different SSP scenarios compared to the ensemble average. One of the reasons for the lower ET increase is that although the future rise in temperature may accelerate evapotranspiration, increased CO₂ concentration and increased humidity (caused by increased rainfall intensity) may inhibit transpiration by altering leaf stomata, potentially offsetting the increased rate of evapotranspiration, which is also reported in other studies (Snyder *et al.* 2011; Chanapathi *et al.* 2018). The lower ET demand in the future period, combined with the higher precipitation, will lead to higher runoff generation from the basin. The percentage change of WBC is continuously increasing from NF to FF under all scenarios except for SSP1-2.6. In the case of SSP1-2.6, the percentage change of WBC (except streamflow) is higher than MF and FF.

The relative change calculated between the historical GCM ensemble average and future GCM ensemble average was applied to IMD observed values of the baseline period to obtain the expected future WBCs (see Table S8, Supplementary material). The average annual precipitation is expected to increase in the range of 781–1,072 mm for future periods under different SSP scenarios based on IMD data. In a similar way, future predictions indicate that surface runoff, water yield, evapotranspiration and streamflow range from 104 to 184 mm, 155 to 268 mm, 540 to 610 mm, and 920 to 1,506 m³/s, respectively, for different scenarios.

A further analysis was performed to evaluate the climate change impacts during the Indian summer monsoon rainfall (ISMR: from June to October) period. The prediction ranges of various GCMs and their ensemble averages compared with the GCM historical baseline period are given in Tables 5 and 6, respectively.

It can be found that nearly 90% of the climate change impact on WBC is occurring in the ISMR period. This study mainly focused on precipitation, water yield and surface runoff. It can be observed that there are significant variations in all WBCs from the prediction bound values. The ensemble mean of precipitation varies from a minimum of 129 mm (under GCM: NorESM1-LM) to a maximum of 2,569 mm (under GCM: IPSL-CM6A-LR) in the future (Table 5). From the ensemble average, it can be observed that almost all the scenarios show a similar kind of increase in precipitation in the near future. The ensemble average of ISMR precipitation is projected to increase in the range of 13.7–55% for the future period compared to the historical GCM ensemble average of the baseline period. The maximum increases in the ensemble average precipitation are observed as 19, 28.3, 43 and 55%, respectively, in the far future under SSP1-2.6, SSP2-4.5, SSP3-7.0, and SSP5-8.5

Table 5 | Impact of climate change on the WBC for KRB with prediction bounds for annual average ISMR

	Precipitation (mm)	ET (mm)	Water yield (mm)	Surface runoff (mm)	Streamflow (m ³ /s)
IMD	600	366	110	79	1,659
GCM historical	724	314	259	156	4,026
SSP1-2.6 (NF)	857 (186–2,148)	329 (155–476)	369 (22–1,569)	213 (13–834)	5,268 (830–16,592)
SSP1-2.6 (MF)	849 (251–1,875)	330 (191–429)	362 (20–1,280)	209 (10–707)	5,271 (87–14,667)
SSP1-2.6 (FF)	862 (220–1,811)	336 (176–434)	364 (12–1,231)	209 (6–678)	5,316 (30–13,401)
SSP2-4.5 (NF)	823 (289–1,742)	328 (205–428)	337 (19–1,102)	197 (12–617)	4,929 (149–12,337)
SSP2-4.5 (MF)	907 (129–1,846)	334 (116–443)	403 (11–1,263)	236 (3–751)	5,815 (235–13,254)
SSP2-4.5 (FF)	928 (311–2,187)	341 (196–464)	418 (40–1,588)	243 (23–963)	6,062 (407–16,467)
SSP3-7.0 (NF)	848 (167–1,873)	333 (149–435)	357 (12–1,231)	208 (7–709)	5,221 (536–14,045)
SSP3-7.0 (MF)	898 (347–1,887)	336 (238–457)	397 (40–1,303)	238 (25–760)	5,805 (350–15,315)
SSP3-7.0 (FF)	1,037 (184–1,986)	354 (151–459)	505 (16–1,474)	303 (7–819)	7,155 (828–16,236)
SSP5-8.5 (NF)	836 (215–1,847)	328 (181–431)	348 (13–1,273)	202 (7–683)	4,966 (135–12,667)
SSP5-8.5 (MF)	937 (137–1,745)	338 (114–438)	423 (16–1,114)	251 (9–718)	6,083 (222–12,958)
SSP5-8.5 (FF)	1,123 (130–2,569)	356 (105–453)	576 (9–1,980)	347 (4–1,450)	8,009 (1,323–20,382)

Table 6 | Percentage deviation (in parentheses) of WBC due to climate change over KRB for ISMR season

	Precipitation (mm)	ET (mm)	Water yield (mm)	Surface runoff (mm)	Streamflow (m ³ /s)
GCM historical	724	314	259	156	4,026
SSP1-2.6 (NF)	857 (18.4)	329 (4.8)	369 (42.5)	213 (36.5)	5,268 (30.8)
SSP1-2.6 (MF)	849 (17.3)	330 (5.1)	362 (39.7)	209 (34)	5,271 (31)
SSP1-2.6 (FF)	862 (19)	336 (7)	364 (40.5)	209 (34)	5,316 (32)
SSP2-4.5 (NF)	823 (13.7)	328 (4.5)	337 (30)	197 (26.3)	4,929 (22.5)
SSP2-4.5 (MF)	907 (25.3)	334 (6.5)	403 (55.6)	236 (51.3)	5,815 (44.2)
SSP2-4.5 (FF)	928 (28.3)	341 (8.6)	418 (61.4)	243 (55.8)	6,062 (50.6)
SSP3-7.0 (NF)	848 (17)	333 (6)	357 (37.8)	208 (33.33)	5,221 (30)
SSP3-7.0 (MF)	898 (24)	336 (7)	397 (53.3)	238 (52.5)	5,805 (44.2)
SSP3-7.0 (FF)	1,037 (43)	354 (12.7)	505 (95)	303 (94)	7,155 (77.7)
SSP5-8.5 (NF)	836 (15.5)	328 (4.5)	348 (34.4)	202 (29.5)	4,966 (23)
SSP5-8.5 (MF)	937 (29.5)	338 (7.6)	423 (63.3)	251 (61)	6,083 (51.1)
SSP5-8.5 (FF)	1,123 (55)	356 (13.4)	576 (122.4)	347 (122)	8,009 (99)

(Table 6). The increases in precipitation are larger under SSP5-8.5 and SSP3-7.0 than under the other scenarios. The direct response of water yield and surface runoff to the precipitation also follows the same trend as the precipitation. The surface runoff and water yield components are anticipated to increase up to 175 and 245 mm for the ISMR period and 184 and 268 mm for the annual period, respectively, by the end of the 21st century under the SSP 5-8.5 scenario after applying the relative percentage of GCMs to the IMD observed values (see Table S9, Supplementary material). Almost 95% of the annual surface runoff and 92% of annual water yield occur during the ISMR period. This is due to a higher occurrence of precipitation during the monsoon period. Generally, the rise in the WBC may indicate excessive availability of water and high groundwater storage. The streamflow is expected to increase significantly in the future under all the scenarios. The individual streamflow for one of the GCMs is projected to experience a maximum increase of up to $20,382 \text{ m}^3/\text{s}$ under the SSP5-8.5 scenario in the FF period. The selected SSP scenarios showed an increase in surface runoff, water yield and streamflow due to increasing rainfall. The evapotranspiration also follows an increasing trend but a lesser increase than the other WBCs under all SSP scenarios. These results are similar to those reported in earlier studies (Kulkarni *et al.* 2014; Chanapathi *et al.* 2018). The ensemble mean of ISMR future streamflow ranges from 4,929 to $8,009 \text{ m}^3/\text{s}$ under different SSP scenarios, which is 22.5–99% more than the historical GCM ensemble average. The results suggest that more water will be available in the basin in the future and the basin may experience more floods.

The impact of climate change was also assessed by comparing the mean monthly streamflow for the future periods with the baseline period, as shown in Figure 11. It is clearly observed that, compared to the baseline period, future streamflow is significantly higher (particularly with higher variations from June to October) under all scenarios. During the NF period, the output of the NorESM2-LM GCM projects a higher magnitude of streamflow compared to the outputs of other GCMs under four SSP scenarios. It is observed that the maximum flow value reaches $13,213 \text{ m}^3/\text{s}$ in August for the SSP1-2.6 scenario. For the MF period, the EC-EARTH3 output projects a higher magnitude of streamflow under the SSP3-7.0 scenario with a streamflow value of about $13,102 \text{ m}^3/\text{s}$ in August. Likewise, in the FF period, EC-EARTH3-VEG shows a large magnitude of streamflow under the SSP5-8.5 scenario with a peak flow of $15,166 \text{ m}^3/\text{s}$ in September.

It can be observed that there is a shift in the occurrence of peak flow value in the future period compared to the observed period 1973–2003. In the observed period, the highest recorded flow rate was $2,540 \text{ m}^3/\text{s}$, which took place during August.

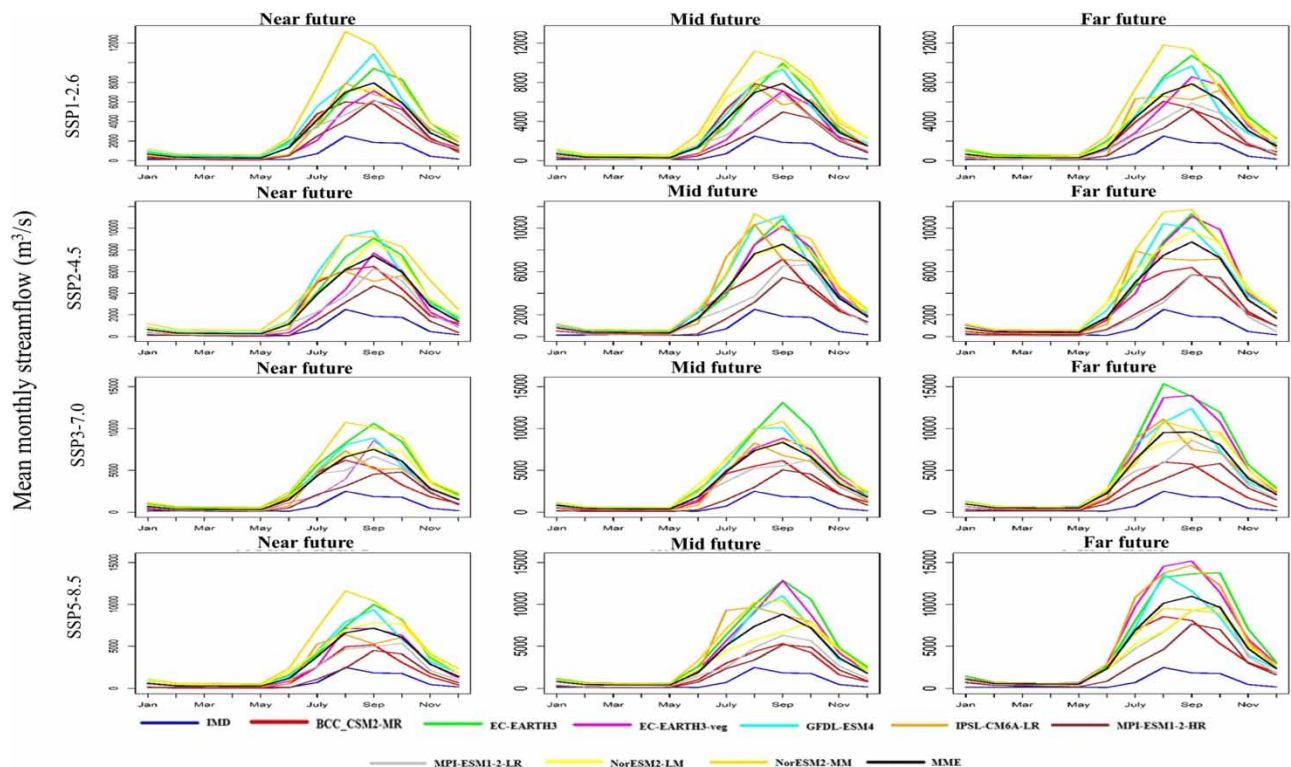


Figure 11 | Simulated mean monthly streamflow under different SSP scenarios in the future periods.

However, in the future periods, the peak flow values for most of the individual GCMs and MME averages were observed in September. For the EC-EARTH3 model, the peak flow value is projected to occur in October in FF under the SSP5-8.5 scenario. This shift in peak streamflow in future periods compared to the observed period can be related to the extension of ISMR even up to October, resulting in an increase in surface runoff. This significant surface runoff in September and October negatively impacts the Kharif crops in the KRB since most of the crops are in the harvesting stage, particularly rice, maize and cotton. It can be observed that the streamflow increment is more in MF and FF than in NF under all SSP scenarios except the SSP1-2.6 scenario. Under the SSP1-2.6 scenario, the highest MME average streamflow in the NF is predicted to rise about 3.17 times (i.e., 7,942 m³/s) compared to that in the historical period (i.e., 2,540 m³/s). Likewise, the projected increases in maximum MME average streamflow during the MF and FF under SSP5-8.5 are estimated to be 3.52 (8,835.9 m³/s) and 4.38 (10,973 m³/s) times, respectively, compared to the baseline period. These findings align with previous studies (Nikam *et al.* 2018; Chanapathi & Thatikonda 2020).

4.4. Streamflow extremes

Meteorological anomalies within the basin contribute to the hydrological extremes such as floods and droughts over a catchment. It can be seen that inter-annual variations in streamflow (see Figure 10) are increasing in the future periods under all scenarios compared to observed flows, indicating that extremes may be increasing. The projected changes in the hydrological extremes were analysed by flood frequency analysis of the annual maximum discharge for the flow at the watershed outlet. The floods of different return periods (T_p : 25, 50, 75 and 100 years) were estimated using General Extreme Value type-1 Gumbel distribution (Gumbel 1941). Hydrological extremes are defined as floods having magnitudes equal to or greater than these return period events. Analysis was carried out to count the number of extreme events during future periods of chosen GCMs and their magnitudes for 25-, 50-, 75- and 100-year return periods under four scenarios (Table 7). It can be observed

Table 7 | Number of probable flood extremes in the KRB under NF, MF and FF for future scenarios

		1	2	3	4	5	6	7	8	9
Return period (T_p)	Flood in (m³/s)	Count of extremes (NF, MF, FF)								
SSP1-2.6										
25	26,845	6,6,0	15,25,6	0,0,3	7,3,16	35,24,16	0,0,0	2,1,0	86,54,95	2,0,8
50	31,039	0,0,0	8,3,2	0,0,0	3,2,10	28,17,8	0,0,0	0,0,0	42,11,42	0,0,0
75	33,477	0,0,0	1,0,2	0,0,0	2,0,7	26,13,8	0,0,0	0,0,0	29,4,31	0,0,0
100	35,202	0,0,0	0,0,0	0,0,0	0,0,5	25,10,5	0,0,0	0,0,0	21,1,20	0,0,0
SSP2-4.5										
25	26,845	0,11,3	2,27,31	10,33,10	0,34,12	28,110,71	0,0,0	0,4,0	24,58,88	11,1,9
50	31,039	0,3,0	0,12,15	1,10,0	0,8,9	16,64,48	0,0,0	0,0,0	2,16,43	0,0,1
75	33,477	0,2,0	0,5,7	0,4,0	0,6,7	12,39,26	0,0,0	0,0,0	0,13,33	0,0,0
100	35,202	0,0,0	0,4,7	0,3,0	0,3,3	10,29,19	0,0,0	0,0,0	0,12,30	0,0,0
SSP3-7.0										
25	26,845	0,1,0	10,50,164	0,13,138	11,0,49	32,40,91	0,0,0	0,0,2	57,44,89	5,9,18
50	31,039	0,0,0	7,11,82	0,4,90	5,0,18	18,20,67	0,0,0	0,0,0	24,18,31	3,0,0
75	33,477	0,0,0	5,8,46	0,2,75	1,0,11	11,6,56	0,0,0	0,0,0	18,7,17	1,0,0
100	35,202	0,0,0	2,7,33	0,1,65	0,0,8	7,5,51	0,0,0	0,0,0	14,2,14	1,0,0
SSP5-8.5										
25	26,845	0,7,35	3,34,138	4,45,209	12,4,94	47,94,214	0,0,0	14,0,6	35,70,49	11,0,10
50	31,039	0,4,18	0,10,88	0,25,112	3,0,34	29,61,132	0,0,0	9,0,0	17,32,23	8,0,2
75	33,477	0,2,12	0,7,61	0,14,78	1,0,22	20,44,101	0,0,0	4,0,0	11,24,10	7,0,0
100	35,202	0,1,12	0,6,50	0,10,63	0,0,12	18,33,88	0,0,0	2,0,0	2,9,4	6,0,0

Note: 1–9 indicates GCM 1–9 representing BCC-CSM2-MR, EC-Earth3, EC-Earth3-Veg, GFDL-ESM4, IPSL-CM6A-LR, MPI-ESM1-2-HR, MPI-ESM1-2-LR, NorESM2-LM, and NorESM2-MM, respectively.

that the frequency of extreme events significantly increases from NF to FF and the magnitude of these events also increases. The maximum number of extremes can be seen for NorESM2-LM, followed by IPSLCM-6A-LR, EC-EARTH3, EC-EARHT3-VEG, GFDL-ESM4, NorEM2-MM, BCC-ESM-MR and MPI-ESM1-2-LR under different scenarios. MPI-ESM1-2-HR does not show any extreme events in the future. The highest number of hydrological extremes of the 100-year return period is observed as 88 in 25 years for IPSL-CM6A-LR under SSP5-8.5 in FF. The maximum heavy floods of future periods for different return periods vary from 47,700 to 85,690 m³/s. These values are very high compared to previous floods (1998, 2005, 2006 and 2009 year floods) in the KRB, and the increment ranges from 1.72 to 3.1 times the highest flood (27,660 m³/s) that occurred in the year 2009 (Central Water Commission 2019). The analysis of the extreme flood events would help manage the water resources and is very useful for various stakeholders in planning and designing different hydraulic structures.

4.5. DISCUSSION

The research on the KRB is of utmost importance due to its semi-arid environment and susceptibility to climate change, resulting from an uneven spread of rainfall. Previous research has suggested that choosing appropriate GCMs can help to decrease uncertainties in climate change projections (Raju & Nagesh kumar 2014; McSweeney *et al.* 2015). The selected GCMs using the SU technique agree with the previous studies of different CMIP phases over the KRB. The NorESM and BCCCSM1.1 families of GCMs secured the top rank in evaluating ISMR (Babar *et al.* 2015; Parth Sarthi *et al.* 2016). The GFDL and BCCR families of GCMs secured the top rank in evaluating the precipitation in the KRB (Raju & Nagesh Kumar 2015), and the IPSL family performs well for the temperature over India (Raju & Nagesh Kumar 2016). The NorESM, BCCCSM1.1, GFDL, BCCR and IPSL families GCMs are ranked in the top 50% in the present study. However, for the CMIP6 phase climate models, the MPI family performs than other GCMs, which agrees with models for the whole Indian peninsular (Anandhi & Nanjundiah 2015). Therefore, the selected top 50% GCMs were utilised to compel the hydrologic SWAT model. The average annual precipitation of the MME average, along with individual GCM, significantly increases from IMD precipitation in all three future periods; this is in contrast with a previous study, which reported decreasing precipitation projections in the NF using the GHG (Gosain *et al.* 2006), CNRM-CM5 and GFDL-ESM2M GCM (Chanapathi & Thatikonda 2020) outputs.

The increase in the precipitation resulted in an increase of other WBCs, such as surface runoff, water yield and streamflow, and a decrease in evapotranspiration in the future can be observed in the present study. The results align with previous studies (Kulkarni *et al.* 2014; Kundu *et al.* 2017; Nikam *et al.* 2018; Chanapathi & Thatikonda 2020). For example, the maximum amount of annual average precipitation was projected to increase by about 33.4% under CNRM-CM5 output in FF under the high-emission RCP8.5 scenario (Chanapathi & Thatikonda 2020) compared to the baseline period, whereas in the present study, the MME average is projected to increase about 54% in FF under the SSP5-8.5 scenario. Ensemble average precipitation was projected to increase up to 1,073 mm under the RCP8.5 scenario, whereas in the present study, it is projected to increase up to 1,187 mm under the SSP5-8.5 scenario in the FF. Similarly, the ensemble average values of water yield, surface runoff and streamflow were projected to increase up to 499 mm, 459 mm and 6,021 m³/s, whereas, in the current study, these are projected to increase up to 609 mm, 354 mm and 4,226 m³/s in the FF, respectively. The lower increase in streamflow and surface runoff could be attributed to the incorporation of the reservoir system into the SWAT model. The results of the study suggest that future policies for cropping patterns, cropping periods and reservoir operations must be updated for sustainable water management within the basin. According to Nikam *et al.* (2018), the number of extreme streamflow events is expected to increase up to 289 for the 100-year return period over a 20-year period, whereas in the present study, the probability of extreme streamflow events for the same return period is projected to be about 88 times for MF.

5. SUMMARY AND CONCLUSIONS

This study examines the impacts of climate change on the WBCs and hydrology of the KRB for three future time frames. Tier-1 scenarios, SSP1-2.6, SSP2-4.5, SSP3-7.0 and SSP5-8.5, which are similar in magnitude and distribution to the RCPs in CMIP5, were used in the current study. The future scenarios of the selected top 50% GCMs were forced as input to the well-calibrated and validated distributed hydrological model (SWAT) to simulate the WBCs and streamflow. Significant changes were observed for hydrological components in annual and ISMR periods. The future flood frequency analysis of different return periods (25, 50, 75 and 100 years) was carried out using Gumbel distribution over the observed period. Based on these flood extremes, the future hydrological extremes were identified. The following are the key findings of the study.

The MPI-ESM1-2-HR and MPI-ESM1-2-LR GCMs closely matched observed precipitation data during the baseline period, with no significant changes expected in the future except under the SSP5-8.5 scenario during the FF period. The outputs of NorESM2-LM and NorESM2-MM GCMs consistently overestimated future precipitation across all SSP scenarios except in the FF under the SSP5-8.5 scenario. It was observed that the ensemble mean of projected mean annual precipitation significantly increased in the range of 12–54% in the future periods under different SSP scenarios compared to the GCM ensemble. The fluctuation of these predicted precipitation levels will likely have a significant impact on other WBCs in the basin. The ensemble average of annual surface runoff and water yield is projected to increase from 27 to 124% and from 30 to 125%, respectively, under different SSP scenarios for future periods. With the increase in precipitation, ET is also projected to increase under all scenarios in the future periods, but the percentage increase of ET is less than the baseline period ET and the other WBCs in the future. The future streamflow is significantly impacted by changes in future precipitation, and the annual MME average is projected to increase from 31 to 114.5% from NF to FF under four SSP scenarios. The ensemble mean of future flows occurred mostly in September, and the increase in flows can also be observed even in October and November due to monsoon extension. This shows the adverse effects on Kharif crops as these are in the harvesting stage. Policymakers can decide on cropping patterns and cultivation for better agricultural productivity. Future streamflow is significantly impacted by the large increases in precipitation, surface runoff and water yield, which may result in major flood events in the KRB. A significant increase in the monthly flows can be observed for the NF to FF compared to that for the baseline period. Compared to the non-monsoon period, the maximum peak flows are observed during the monsoon period. It is found that the MPI-ESM1-2-HR model will not experience any extreme flow occurrences in the future. The maximum number of streamflow extremes can be observed for NorESM2-LM and IPSL-CM6A-LR outputs. More probable extreme flood events are observed under SSP5-8.5 in the far future for all the return periods. The projected maximum heavy floods in future periods range from 1.72 to 3.1 times the highest recorded flood of 27,660 m³/s in 2009. This information could be very beneficial for reservoir operations in the KRB. Therefore, it may be concluded that there are more water availability chances in the KRB under different CMIP6 climate change projections and also there is a probability of floods in future periods. As a result, this knowledge is beneficial for sustainable development and improved planning and management of water resources.

The climate change impact on the hydrological analysis of the WBC of the catchment is mostly affected by the uncertainties in the climate projections and hydrological model itself. The individual GCM results and their minimum and maximum bounds also show the uncertainties associated with selected projections. The MPI-ESM1-2-HR and MPI-ESM1-2-LR GCMs secured the first and second ranks and had shown less uncertainty range in the future projections compared to other GCMs. The present study also tried to reduce the uncertainty in climate projections by making an ensemble of selected GCMs. Even though the hydrological model is calibrated and validated, the uncertainty may still exist, which can be reduced to some extent by employing an ensemble of hydrological models (Wolock & McCabe 1999; Arnell & Liv 2001). The present study considered historical LULC for future climate change projections; however, alterations in land use, soil composition, management practices and other climate factors will also have a significant impact on both water availability and crop production. The present study results can be improved by employing future land use with respect to the different climate projections. Finally, the results presented here are very helpful to the decision makers for better planning and management of water resources in the basin.

DATA AVAILABILITY STATEMENT

All relevant data are available from an online repository or repositories. For Meteorological data of observed datasets use Indian Metrological Department (IMD; <https://www.imdpune.gov.in/>). The GCM data can be downloaded from Earth System Grid Federation (ESGF) portal (<https://esgf-node.llnl.gov/search/cmip6>)

CONFLICT OF INTEREST

The authors declare there is no conflict.

REFERENCES

- Abbaspour, K. C., Rouholahnejad, E., Vaghefi, S., Srinivasan, R., Yang, H. & Klöve, B. 2015 A continental-scale hydrology and water quality model for Europe: Calibration and uncertainty of a high-resolution large-scale SWAT model. *Journal of Hydrology* **524**, 733–752. <https://doi.org/https://doi.org/10.1016/j.jhydrol.2015.03.027>.

- Ahmed, K., Shahid, S., Sachindra, D. A., Nawaz, N. & Chung, E.-S. 2019 Fidelity assessment of general circulation model simulated precipitation and temperature over Pakistan using a feature selection method. *Journal of Hydrology* **573**, 281–298. <https://doi.org/10.1016/j.jhydrol.2019.03.092>.
- Ahmed, K., Sachindra, D. A., Shahid, S., Iqbal, Z., Nawaz, N. & Khan, N. 2020 Multi-model ensemble predictions of precipitation and temperature using machine learning algorithms. *Atmospheric Research* **236**, 104806. <https://doi.org/10.1016/j.atmosres.2019.104806>.
- Anandhi, A. & Nanjundiah, R. S. 2015 Performance evaluation of AR4 climate models in simulating daily precipitation over the Indian region using skill scores. *Theoretical and Applied Climatology* **119** (3), 551–566. <https://doi.org/10.1007/s00704-013-1043-5>.
- Anil, S. & Anand Raj, P. 2022 Deciphering the projected changes in CMIP-6 based precipitation simulations over the Krishna River Basin. *Journal of Water and Climate Change* **13** (3), 1389–1407. <https://doi.org/10.2166/wcc.2022.399>.
- Anil, S., Manikanta, V. & Pallakury, A. R. 2021 Unravelling the influence of subjectivity on ranking of CMIP6 based climate models: A case study. *International Journal of Climatology*. November 2020. <https://doi.org/10.1002/joc.7164>.
- Arnell, N. W. & Liv, C. 2001 Hydrology and water resources. In: McCarthy, J.J., Canziani, O.F., Leary, N.A., Dokken, D.J. and White, K.S. (eds.) *Climate Change 2001: Impacts, Adaptation and Vulnerability*. Cambridge, UK. Cambridge University Press, pp. 191–233.
- Arnold, J. G., Moriasi, D. N., Gassman, P. W., Abbaspour, K. C., White, M. J., Srinivasan, R., Santhi, C., Harmel, R. D., van Griensven, A., Van Liew, M. W., Kannan, N. & Jha, M. K. 2012 SWAT: Model use, calibration, and validation. *Transactions of the ASABE* **55** (4), 1491–1508. <https://doi.org/10.13031/2013.42256>.
- Babar, Z. A., Zhi, X. F. & Fei, G. 2015 Precipitation assessment of Indian summer monsoon based on CMIP5 climate simulations. *Arabian Journal of Geosciences* **8** (7), 4379–4392. <https://doi.org/10.1007/s12517-014-1518-4>.
- Bandyopadhyay, A., Nengzouam, G., Singh, W. R., Hangsing, N. & Bhadra, A. 2018 Comparison of various reanalyses gridded data with observed data from meteorological stations over India. **3**, 190–180. <https://doi.org/10.29007/c1sf>.
- Bhatta, B., Shrestha, S., Shrestha, P. K. & Talchabhadel, R. 2019 Evaluation and application of a SWAT model to assess the climate change impact on the hydrology of the Himalayan River Basin. *CATENA* **181** (May), 104082. <https://doi.org/10.1016/j.catena.2019.104082>.
- Central Water Commission 2019 *Morphological Study of Krishna and Tungabhadra Basins Using Remote Sensing Technique*. Funded by Ministry of Water Resources Government of India.
- Chanapathi, T. & Thatikonda, S. 2020 Investigating the impact of climate and land-use land cover changes on hydrological predictions over the Krishna river basin under present and future scenarios. *Science of the Total Environment* **721**, 137736. <https://doi.org/10.1016/j.scitotenv.2020.137736>.
- Chanapathi, T., Thatikonda, S. & Raghavan, S. 2018 Analysis of rainfall extremes and water yield of Krishna River Basin under future climate scenarios. *Journal of Hydrology: Regional Studies* **19** (June), 287–306. <https://doi.org/10.1016/j.ejrh.2018.10.004>.
- Chen, H., Xu, C.-Y. & Guo, S. 2012 Comparison and evaluation of multiple GCMs, statistical downscaling and hydrological models in the study of climate change impacts on runoff. *Journal of Hydrology* **434–435**, 36–45. <https://doi.org/10.1016/j.jhydrol.2012.02.040>.
- Chiew, F. H. S., Teng, J., Vaze, J. & Kirono, D. G. C. 2009 Influence of global climate model selection on runoff impact assessment. *Journal of Hydrology* **379** (1–2), 172–180. <https://doi.org/10.1016/j.jhydrol.2009.10.004>.
- Das, A., Krishnaswami, S., Sarin, M. M. & Pande, K. 2005 Chemical weathering in the Krishna Basin and Western Ghats of the Deccan Traps, India: Rates of basalt weathering and their controls. *Geochimica et Cosmochimica Acta* **69** (8), 2067–2084. <https://doi.org/10.1016/j.gca.2004.10.014>.
- Eisner, S., Voss, F. & Kynast, E. 2012 Statistical bias correction of global climate projections – consequences for large scale modeling of flood flows. *Advances in Geosciences* **31**, 75–82. <https://doi.org/10.5194/adgeo-31-75-2012>.
- Eyring, V., Bony, S., Meehl, G. A., Senior, C. A., Stevens, B., Stouffer, R. J. & Taylor, K. E. 2016 Overview of the Coupled Model Intercomparison Project Phase 6 (CMIP6) experimental design and organization. *Geoscientific Model Development* **9** (5), 1937–1958. <https://doi.org/10.5194/gmd-9-1937-2016>.
- Faye, C. 2022 Comparative analysis of meteorological drought based on the SPI and SPEI indices. *HighTech and Innovation Journal* **3**, 15–27. <https://doi.org/10.28991/HIJ-SP2022-03-02>.
- Gao, H., Sabo, J. L., Chen, X., Liu, Z., Yang, Z., Ren, Z. & Liu, M. 2018 Landscape heterogeneity and hydrological processes: A review of landscape-based hydrological models. *Landscape Ecology* **33** (9), 1461–1480. <https://doi.org/10.1007/s10980-018-0690-4>.
- Gidden, M. J., Riahi, K., Smith, S. J., Fujimori, S., Luderer, G., Kriegler, E., Van Vuuren, D. P., Van Den Berg, M., Feng, L., Klein, D., Calvin, K., Doelman, J. C., Frank, S., Fricko, O., Harmsen, M., Hasegawa, T., Havlik, P., Hilaire, J., Hoesly, R. & Takahashi, K. 2019 Global emissions pathways under different socioeconomic scenarios for use in CMIP6: A dataset of harmonized emissions trajectories through the end of the century. *Geoscientific Model Development* **12** (4), 1443–1475. <https://doi.org/10.5194/gmd-12-1443-2019>.
- Githui, F., Gitau, W., Mutua, F. & Bauwens, W. 2009 Climate change impact on SWAT simulated streamflow in western Kenya. *International Journal of Climatology* **29** (12), 1823–1834. <https://doi.org/10.1002/joc.1828>.
- Gleckler, P. J., Taylor, K. E. & Doutriaux, C. 2008 Performance metrics for climate models. *Journal of Geophysical Research: Atmospheres* **113** (D6). <https://doi.org/10.1029/2007JD008972>.
- Gong, D. Y., Shi, P. J. & Wang, J. A. 2004 Daily precipitation changes in the semi-arid region over northern China. *Journal of Arid Environments* **59** (4), 771–784. <https://doi.org/10.1016/j.jaridenv.2004.02.006>.
- Gosain, A. K., Rao, S. & Basuray, D. 2006 Climate change impact assessment on hydrology of Indian river basins. *Current Science* **90** (3), 346–353.

- Gosain, A. K., Rao, S., Arora, A. 2011 Climate change impact assessment of water resources of India. *Current Science* **101** (3), 356–371.
- Gouda, K. C., Nahak, S. & Goswami, P. 2018 [Evaluation of a GCM in seasonal forecasting of extreme rainfall events over continental India. *Weather and Climate Extremes* **21** \(September\), 10–16. <https://doi.org/10.1016/j.wace.2018.05.001>.](#)
- Gumbel 1941 [Probability-interpretation of the observed return-periods of floods. *Eos, Transactions American Geophysical Union* **22** \(3\), 836–850. <https://doi.org/https://doi.org/10.1029/TR022i003p00836>.](#)
- Gusain, A., Ghosh, S. & Karmakar, S. 2020 [Added value of CMIP6 over CMIP5 models in simulating Indian summer monsoon rainfall. *Atmospheric Research* **232**, 104680. <https://doi.org/https://doi.org/10.1016/j.atmosres.2019.104680>.](#)
- Hang, N. P. T. 2022 [Policy implications for the green bank development in the context of global climate change. *Emerging Science Journal* **6** \(4\), 817–833. <https://doi.org/10.28991/ESJ-2022-06-04-011>.](#)
- Hassan, I., Kalin, R. M., White, C. J. & Aladejana, J. A. 2020 Selection of CMIP5 GCM ensemble for the projection of Spatio-temporal changes in precipitation and temperature over the Niger Delta, Nigeria. *Water* **12** (2), 385.
- Homsai, R., Shiru, M. S., Shahid, S., Ismail, T., Harun, S. B., Al-Ansari, N., Chau, K.-W. & Yaseen, Z. M. 2020 [Precipitation projection using a CMIP5 GCM ensemble model: A regional investigation of Syria. *Engineering Applications of Computational Fluid Mechanics* **14** \(1\), 90–106. <https://doi.org/10.1080/19942060.2019.1683076>.](#)
- IPCC 2013 AR5 – Citations. *Climate Change 2013 – The Physical Science Basis, Contribution of Working Group I to the Fifth Assessment Report of the Intergovernmental Panel on Climate Change*, 3. <https://doi.org/10.1017/CBO9781107415324.Summary>
- Iqbal, Z., Shahid, S., Ahmed, K., Ismail, T., Khan, N., Virk, Z. T. & Johar, W. 2020 [Evaluation of global climate models for precipitation projection in sub-Himalaya region of Pakistan. *Atmospheric Research* **245**, 105061. <https://doi.org/10.1016/j.atmosres.2020.105061>.](#)
- Khan, N., Shahid, S., Ahmed, K., Ismail, T., Nawaz, N. & Son, M. 2018 [Performance assessment of general circulation model in simulating daily precipitation and temperature using multiple gridded datasets. *Water* **10** \(12\), 1793. <https://doi.org/10.3390/w10121793>.](#)
- Knutti, R., Abramowitz, G., Collins, M., Eyring, V., Gleckler, P. J., Hewitson, B. & Mearns, L. 2010 Good Practice Guidance Paper on Assessing and Combining Multi Model Climate Projections. In: *IPCC Expert Meeting on Assessing and Combining Multi Model Climate Projections*, p. 15.
- Kulkarni, B. D., Deshpande, N. R., Patwardhan, S. K. & Bansod, S. D. 2014 [Assessing hydrological response to changing climate in the Krishna Basin of India. *J. Earth Sci. Clim. Change* **5**, 211. <https://doi.org/10.4172/2157-7617.1000211>.](#)
- Kundu, S., Khare, D. & Mondal, A. 2017 [Individual and combined impacts of future climate and land use changes on the water balance. *Ecological Engineering* **105**, 42–57. <https://doi.org/https://doi.org/10.1016/j.ecoleng.2017.04.061>.](#)
- Latif, M., Hannachi, A. & Syed, F. S. 2018 [Analysis of rainfall trends over indo-Pakistan summer monsoon and related dynamics based on CMIP5 climate model simulations. *International Journal of Climatology* **38**, e577–e595. <https://doi.org/10.1002/joc.5391>.](#)
- Li, Z. & Jin, J. 2017 [Evaluating climate change impacts on streamflow variability based on a multisite multivariate GCM downscaling method in the Jing River of China. *Hydrology and Earth System Sciences* **21** \(11\), 5531–5546. <https://doi.org/10.5194/hess-21-5531-2017>.](#)
- Mann, R. & Gupta, A. 2022 [Temporal trends of rainfall and temperature over two sub-divisions of Western Ghats. *HighTech and Innovation Journal* **3**, 28–42. <https://doi.org/10.28991/HIJ-SP2022-03-03>.](#)
- Maraun, D., Shepherd, T. G., Widmann, M., Zappa, G., Walton, D., Gutiérrez, J. M., Hagemann, S., Richter, I., Soares, P. M. M., Hall, A. & Mearns, L. O. 2017 [Towards process-informed bias correction of climate change simulations. *Nature Climate Change* **7** \(11\), 764–773. <https://doi.org/10.1038/nclimate3418>.](#)
- McMahon, T. A., Peel, M. C. & Karoly, D. J. 2015 *Assessment of Precipitation and Temperature Data From CMIP3 Global Climate Models for Hydrologic Simulation*.
- McSweeney, C. F., Jones, R. G., Lee, R. W. & Rowell, D. P. 2015 [Selecting CMIP5 GCMs for downscaling over multiple regions. *Climate Dynamics* **44** \(11–12\), 3237–3260. <https://doi.org/10.1007/s00382-014-2418-8>.](#)
- Mishra, V. & Lilhare, R. 2016 [Hydrologic sensitivity of Indian sub-continental river basins to climate change. *Global and Planetary Change* **139**, 78–96. <https://doi.org/10.1016/j.gloplacha.2016.01.003>.](#)
- Mishra, V., Bhatia, U. & Tiwari, A. D. 2020 [Bias-corrected climate projections for South Asia from coupled model intercomparison project-6. *Scientific Data* **7** \(1\), 1–13. <https://doi.org/10.1038/s41597-020-00681-1>.](#)
- Moriasi, N. D., Gitau, W., Pai, M. & Daggupati, N. 2015 [Hydrologic and water quality models: Performance measures and evaluation criteria. *Transactions of the ASABE* **58** \(6\), 1763–1785. <https://doi.org/https://doi.org/10.13031/trans.58.10715>.](#)
- Murray, S. J., Foster, P. N. & Prentice, I. C. 2012 [Future global water resources with respect to climate change and water withdrawals as estimated by a dynamic global vegetation model. *Journal of Hydrology* **448–449**, 14–29. <https://doi.org/10.1016/j.jhydrol.2012.02.044>.](#)
- Ndhlovu, G. Z. & Woyessa, Y. E. 2020 [Modelling impact of climate change on catchment water balance, Kabompo River in Zambezi River Basin. *Journal of Hydrology: Regional Studies* **27** \(December 2019\), 100650. <https://doi.org/10.1016/j.ejrh.2019.100650>.](#)
- Neitsch, S., Arnold, J., Kiniry, J. & Williams, J. 2011 *Soil & Water Assessment Tool Theoretical Documentation Version 2009*. Texas Water Resources Institute, pp. 1–647. <https://doi.org/10.1016/j.scitotenv.2015.11.063>.
- Nikam, B. R., Garg, V., Jeyaprakash, K., Gupta, P. K., Srivastav, S. K., Thakur, P. K. & Aggarwal, S. P. 2018 [Analyzing future water availability and hydrological extremes in the Krishna basin under changing climatic conditions. *Arabian Journal of Geosciences* **11** \(19\). <https://doi.org/10.1007/s12517-018-3936-1>.](#)
- Noor, M., Ismail, T., Shahid, S., Nashwan, M. S. & Ullah, S. 2019 [Development of multi-model ensemble for projection of extreme rainfall events in Peninsular Malaysia. *Hydrology Research* **50** \(6\), 1772–1788. <https://doi.org/10.2166/nh.2019.097>.](#)

- O'Neill, B. C., Tebaldi, C., Van Vuuren, D. P., Eyring, V., Friedlingstein, P., Hurtt, G., Knutti, R., Kriegler, E., Lamarque, J. F., Lowe, J., Meehl, G. A., Moss, R., Riahi, K. & Sanderson, B. M. 2016 *The Scenario Model Intercomparison Project (ScenarioMIP) for CMIP6. Geoscientific Model Development* **9** (9), 3461–3482. <https://doi.org/10.5194/gmd-9-3461-2016>.
- Pai, D. S., Sridhar, L., Rajeevan, M., Sreejith, O. P., Satbhai, N. S. & Mukhopadhyay, B. 2014 *Development of a new high spatial resolution (0.25× 0.25) long period (1901–2010) daily gridded rainfall data set over India and its comparison with existing data sets over the region. Mausam* **65** (1), 1–18.
- Pandey, B. K., Khare, D., Kawasaki, A. & Mishra, P. K. 2019 *Climate change impact assessment on blue and green water by coupling of representative CMIP5 climate models with physical based hydrological model. Water Resources Management* **33** (1), 141–158. <https://doi.org/10.1007/s11269-018-2093-3>.
- Parth Sarthi, P., Kumar, P. & Ghosh, S. 2016 *Possible future rainfall over Gangetic Plains (GP), India, in multi-model simulations of CMIP3 and CMIP5. Theoretical and Applied Climatology* **124** (3–4), 691–701. <https://doi.org/10.1007/s00704-015-1447-5>.
- Perkins, S. E., Pitman, A. J., Holbrook, N. J. & McAneney, J. 2007 *Evaluation of the AR4 climate models' simulated daily maximum temperature, minimum temperature, and precipitation over Australia using probability density functions. Journal of Climate* **20** (17), 4356–4376. <https://doi.org/10.1175/JCLI4253.1>.
- Piani, C., Weedon, G. P., Best, M., Gomes, S. M., Viterbo, P., Hagemann, S. & Haerter, J. O. 2010 *Statistical bias correction of global simulated daily precipitation and temperature for the application of hydrological models. Journal of Hydrology* **395** (3–4), 199–215. <https://doi.org/10.1016/j.jhydrol.2010.10.024>.
- Pierce, D. W., Cayan, D. R., Maurer, E. P., Abatzoglou, J. T. & Hegewisch, K. C. 2015 *Improved bias correction techniques for hydrological simulations of climate change. Journal of Hydrometeorology* **16** (6), 2421–2442. <https://doi.org/10.1175/JHM-D-14-0236.1>.
- Poonia, N. & Azad, S. 2022 *Alpha power exponentiated Teissier distribution with application to climate datasets. Theoretical and Applied Climatology* **149** (1), 339–353. <https://doi.org/10.1007/s00704-022-04039-y>.
- Pour, S. H., Shahid, S., Chung, E. S. & Wang, X. J. 2018 *Model output statistics downscaling using support vector machine for the projection of spatial and temporal changes in rainfall of Bangladesh. Atmospheric Research* **213** (December 2017), 149–162. <https://doi.org/10.1016/j.atmosres.2018.06.006>.
- Raju, K. S. & Nagesh kumar, D. 2014 *Ranking of global climate models for India using multicriterion analysis. Climate Research* **60** (2), 103–117.
- Raju, K. S. & Nagesh Kumar, D. 2015 *Ranking general circulation models for India using TOPSIS. Journal of Water and Climate Change* **6** (2), 288–299. <https://doi.org/10.2166/wcc.2014.074>.
- Raju, K. S. & Nagesh Kumar, D. 2016 *Selection of global climate models for India using cluster analysis. Journal of Water and Climate Change* **7** (4), 764–774. <https://doi.org/10.2166/wcc.2016.112>.
- Raju, K. S. & Nagesh Kumar, D. 2020 *Review of approaches for selection and ensembling of GCMs. Journal of Water and Climate Change* **11** (3), 577–599. <https://doi.org/10.2166/wcc.2020.128>.
- Raju, K. S., Sonali, P. & Nagesh kumar, D. 2017 *Ranking of CMIP5-Based Global Climate Models for India Using Compromise Programming*, pp. 563–574. <https://doi.org/10.1007/s00704-015-1721-6>.
- Ramesh, R. & Subramanian, V. 1988 *Temporal, spatial and size variation in the sediment transport in the Krishna River basin, India. Journal of Hydrology* **98** (1), 53–65. [https://doi.org/https://doi.org/10.1016/0022-1694\(88\)90205-3](https://doi.org/https://doi.org/10.1016/0022-1694(88)90205-3).
- Rathinasamy, M., Khosa, R., Adamowski, J., ch, S., Partheepan, G., Anand, J. & Narsimlu, B. 2014 *Wavelet-based multiscale performance analysis: An approach to assess and improve hydrological models. Water Resources Research* **50** (12), 9721–9737. <https://doi.org/10.1002/2013WR014650>.
- Reshmidevi, T. V., Nagesh Kumar, D., Mehrotra, R. & Sharma, A. 2018 *Estimation of the climate change impact on a catchment water balance using an ensemble of GCMs. Journal of Hydrology* **556**, 1192–1204. <https://doi.org/10.1016/j.jhydrol.2017.02.016>.
- Ruan, Y., Yao, Z., Wang, R. & Liu, Z. 2018 *Ranking of CMIP5 GCM skills in simulating observed precipitation over the Lower Mekong Basin, using an improved score-based method. Water* **10** (12). <https://doi.org/10.3390/w10121868>.
- Sahoo, S., Dhar, A., Debsarkar, A. & Kar, A. 2018 *Impact of water demand on hydrological regime under climate and LULC change scenarios. Environmental Earth Sciences* **77** (9), 1–19. <https://doi.org/10.1007/s12665-018-7531-2>.
- Salman, S. A., Shahid, S., Ismail, T. & Wang, X. 2018 *Selection of climate models for projection of spatiotemporal changes in temperature of Iraq with uncertainties. Atmospheric Research*. <https://doi.org/10.1016/j.atmosres.2018.07.008>.
- Shiru, M. S., Shahid, S., Chung, E. S., Alias, N. & Scherer, L. 2019 *A MCDM-based framework for selection of general circulation models and projection of spatio-temporal rainfall changes: A case study of Nigeria. Atmospheric Research* **225**, 1–16. <https://doi.org/10.1016/j.atmosres.2019.03.033>.
- Singh, G. R., Jain, M. K. & Gupta, V. 2019 *Spatiotemporal assessment of drought hazard, vulnerability and risk in the Krishna River basin, India. Natural Hazards* **99** (2), 611–635. <https://doi.org/10.1007/s11069-019-03762-6>.
- Sinha, R. K., Eldho, T. I. & Subimal, G. 2020 *Assessing the impacts of land use/land cover and climate change on surface runoff of a humid tropical river basin in Western Ghats, India. International Journal of River Basin Management* **0** (0), 1–38. <https://doi.org/10.1080/15715124.2020.1809434>.
- Snyder, R. L., Moratell, R., Song, Z., Swelam, A., Jomaa, I. & Shapland, T. 2011 *Evapotranspiration response to climate change. Acta Horticulturae* **922** (May 2021), 91–98. <https://doi.org/10.17660/ActaHortic.2011.922.11>.
- Soro, G. E., Yao, A. B., Kouame, Y. M. & Bi, T. A. G. 2017 *Climate change and its impacts on water resources in the Bandama basin, Côte D'ivoire. Hydrology* **4** (1). <https://doi.org/10.3390/hydrology4010018>.

- Srinivas, C. V., Hariprasad, D., Bhaskar Rao, D. V., Anjaneyulu, Y., Baskaran, R. & Venkatraman, B. 2013 [Simulation of the Indian summer monsoon regional climate using advanced research WRF model](#). *International Journal of Climatology* **33** (5), 1195–1210. <https://doi.org/10.1002/joc.3505>.
- Suman, M. & Maity, R. 2020 [Southward shift of precipitation extremes over south Asia: Evidences from CORDEX data](#). *Scientific Reports* **10** (1), 1–11. <https://doi.org/10.1038/s41598-020-63571-x>.
- Tian, Y., Xu, Y. P., Booij, M. J. & Cao, L. 2016 [Impact assessment of multiple uncertainty sources on high flows under climate change](#). *Hydrology Research* **47** (1), 61–74. <https://doi.org/10.2166/nh.2015.008>.
- Vörösmarty, C. J., McIntyre, P. B., Gessner, M. O., Dudgeon, D., Prusevich, A., Green, P., Glidden, S., Bunn, S. E., Sullivan, C. A., Liermann, C. R. & Davies, P. M. 2010 [Global threats to human water security and river biodiversity](#). *Nature* **467** (7315), 555–561. <https://doi.org/10.1038/nature09440>.
- Wang, S., Kang, S., Zhang, L. & Li, F. 2008 [Modelling hydrological response to different land-use and climate change scenarios in the Zamu River basin of northwest China](#). *Hydrological Processes* **22** (14), 2502–2510. <https://doi.org/10.1002/hyp.6846>.
- Wang, B., Liu, D. L., Macadam, I., Alexander, L. V., Abramowitz, G. & Yu, Q. 2016 [Multi-model ensemble projections of future extreme temperature change using a statistical downscaling method in south eastern Australia](#). *Climatic Change* **138** (1–2), 85–98. <https://doi.org/10.1007/s10584-016-1726-x>.
- Wolock, D. M. & McCabe, G. J. 1999 [Estimates of runoff using water-balance and atmospheric general circulation models1](#). *JAWRA Journal of the American Water Resources Association* **35** (6), 1341–1350. <https://doi.org/10.1111/j.1752-1688.1999.tb04219.x>.
- Xing, W. & Wang, B. 2017 [Predictability and prediction of summer rainfall in the arid and semi-arid regions of China](#). *Climate Dynamics* **49** (1–2), 419–431. <https://doi.org/10.1007/s00382-016-3351-9>.
- Yee, M. S., George, B. A., Nawarathna, B., Malano, H. M. & Parthasaradhi, G. 2009 [Assessing water security across the Krishna River Basin](#). In: *18th World IMACS Congress and MODSIM 2009 – International Congress on Modelling and Simulation: Interfacing Modelling and Simulation with Mathematical and Computational Sciences, Proceedings*, July, pp. 3879–3885.
- Zhang, H. & Huang, G. H. 2013 [Development of climate change projections for small watersheds using multi-model ensemble simulation and stochastic weather generation](#). *Climate Dynamics* **40** (3–4), 805–821. <https://doi.org/10.1007/s00382-012-1490-1>.

First received 3 August 2023; accepted in revised form 4 January 2024. Available online 23 January 2024